

Measurements of OH and RO₂ radicals at Dome C, East Antarctica

A. Kukui^{1,4}, M. Legrand², S. Preunkert², M. M. Frey³, R. Loisil⁵, J. Gil Roca¹, B. Jourdain², M. D. King⁶, J. L. France⁶ and G. Ancellet¹

[1]{LATMOS, CNRS, Paris, France}

[2]{LGGE, CNRS, Grenoble, France}

[3]{BAS, NERC, Cambridge, UK}

[4]{LPC2E, CNRS, Orléans, France}

[5]{ Division Technique, INSU, Meudon, France}

[6] {Department of Earth Sciences, Royal Holloway University of London, Egham, Surrey, UK, TW20 OEX}

Correspondence to: A. Kukui (alexandre.kukui@cnrs-orleans.fr)

Abstract

Concentrations of OH radicals and the sum of peroxy radicals, RO₂, were measured in the boundary layer for the first time on the East Antarctic Plateau at the Concordia Station (Dome C, 75.10° S, 123.31° E) during the austral summer 2011/2012. The median concentrations of OH and RO₂ radicals were 3.1×10^6 molecule cm⁻³ and 9.9×10^7 molecule cm⁻³, respectively. These values are comparable to those observed at the South Pole, confirming that the elevated oxidative capacity of the Antarctic atmospheric boundary layer found at the South Pole is not restricted to the South Pole but common over the high Antarctic plateau. At Concordia, the concentration of radicals showed distinct diurnal profiles with the median maximum of 5.2×10^6 molecule cm⁻³ at 11:00 and the median minimum of 1.1×10^6 molecule cm⁻³ at 1:00 for OH radicals and 1.7×10^8 molecule cm⁻³ and 2.5×10^7 molecule cm⁻³ for RO₂ radicals at 13:00 and 23:00, respectively (all times are local times). Concurrent measurements of O₃, HONO, NO, NO₂, HCHO and H₂O₂ demonstrated that the major primary source of OH and RO₂ radicals at Dome C was the photolysis of HONO, HCHO and

H₂O₂, with the photolysis of HONO contributing ~75% of total primary radical production. However, photochemical modelling with accounting for all these radical sources overestimates the concentrations of OH and RO₂ radicals by a factor of 2 compared to field observations. Neglecting the net OH production from HONO in the photochemical modelling results in an underestimation of the concentrations of OH and RO₂ radicals by a factor of 2. To explain the observations of radicals in this case an additional source of OH equivalent to about (25-35)% of measured photolysis of HONO is required. Even with a factor of 5 reduction in the concentrations of HONO, the photolysis of HONO represents the major primary radical source at Dome C. To account for a possibility of an overestimation of NO₂ observed at Dome C the calculations were also performed with NO₂ concentrations estimated by assuming steady state NO₂/NO ratios. In this case the net radical production from the photolysis of HONO should be reduced by a factor of 5 or completely neglected based on the photochemical budget of OH or OD modelling, respectively. Another major factor leading to the large concentration of OH radicals measured at Dome C was large concentrations of NO molecules and fast recycling of peroxy radicals to OH radicals.

1. Introduction

Atmospheric chemistry in polar regions has gained growing interest over the two last decades due to the discovery of surprisingly high photochemical activity in both Antarctic and Arctic, i.e. at the South Pole (Mauldin et al., 2001; Davis et al., 2001) and at Summit, Greenland (Honrath et al., 1999; Sjostedt et al., 2007). The photochemistry of the boundary layer atmosphere (BL) at these snow covered regions is significantly influenced by the emissions of reactive gases from the snowpack. The emissions are produced by the interaction of solar radiation and photo-chemically active species in the snowpack (e.g. Grannas et al., 2007 for a review).

At the South Pole (SP) unexpectedly large concentrations of OH radicals in the boundary layer, about 2×10^6 molecule cm⁻³, were observed for the first time during ISCAT 1998 (Mauldin et al., 2001) and were confirmed in later campaigns (ISCAT 2000 (Mauldin et al., 2004), ANTCI 2003 (Mauldin et al., 2010)). The elevated concentrations of OH radicals were explained by fast recycling of OH radicals from peroxy radicals in presence of large concentrations of NO. The large concentration of NO molecules exceeded free tropospheric concentrations (Davis et al., 2001) and was attributed to the release of NO_x from snowpack

(following UV photolysis of the nitrate anion (NO_3^-) on/in snow grains (Jones et al., 2001)) and its accumulation in a stable and shallow BL at the SP (Davis et al., 2001, 2004, 2008). The build up of large concentrations of NO_x at the SP was suggested to be enhanced by the continuous sunlight during summer and the location at the bottom of a large air drainage basin. (Davis et al., 2004, 2008).

At the SP the major gas-phase net sources of OH and HO_2 radicals were found to be the photolysis of HCHO and H_2O_2 . The production of OH radical from O_3 photolysis was found to be less important owing to the small concentration of water at such low temperatures. The photochemical box model for the SP tends to slightly overpredict the concentrations of OH compared to observations, although satisfactorily reproduces the dependence of the concentration of OH on the concentration of NO (Chen et al., 2004; Mauldin et al., 2004). It has to be emphasized that when considering the mixing ratio of ~ 30 pptv of HONO measured at the SP by using mist chamber/Ion Chromatography method (Dibb et al., 2004) the model overpredicts concentrations of OH radicals at the SP by a factor of 3 to 5 (Chen et al., 2004). It was proposed that the HONO concentrations derived with the mist chamber/Ion Chromatography method during these campaigns were probably biased by some systematic error (e.g., chemical interference) (Chen et al., 2004).

Conditions favouring the accumulation of large concentrations of NO_x were thought to be specific to the South Pole (24 h sunlight and shallow stable boundary layer), however a larger part of Antarctic Plateau also experiences elevated concentrations of NO_x despite strongly reduced solar radiation at night and the resulting build up of an unstable convective atmospheric boundary layer. This is supported by airborne observations of large concentrations of NO (Davis et al., 2008; Slusher et al., 2010) showing that a shallow photochemically active layer is common for large part of Antarctic Plateau atmosphere. However, these airborne measurements of NO_x remain limited in time and space. In addition, although the elevated concentrations of NO_x represent the key factor in build up of large OH concentrations in the polar BL, the relationship of concentrations of OH with concentrations of NO is nonlinear (Mauldin et al., 2004). Thus, an accurate prediction of the concentration of OH radical in other Antarctic regions may be difficult without detailed information on the radical primary production and net losses. These uncertainties in part motivated the OPALE (Oxidant Production in Antarctic Lands and Export) project aiming at a characterisation of the oxidative capacity of the BL atmosphere in the region of East Antarctica.

1 In addition to the monitoring of surface ozone, that was initiated in 2007 at the
2 Concordia station on the East Antarctic plateau (Legrand et al., 2009), two others studies
3 related to the BL photochemistry have been performed at that site prior to the OPALE
4 campaign: The measurements of gas-phase NO concentrations and for the first time on the
5 Antarctic plateau measurements of gas-phase NO₂ concentrations were conducted during
6 summer 2009/2010 by Frey et al. (2013). Frey et al. (2013) revealed that concentrations of
7 NO at Dome C are comparable to those observed at the SP but the ratios [NO₂]/[NO] were
8 found to be significantly larger than calculated assuming photostationary state conditions with
9 measured concentrations of O₃ and NO. As a possible explanation Frey et al. (2013)
10 suggested significantly larger peroxy radical concentrations at Dome C than at the SP. The
11 study of Frey et al., (2013) also revealed a distinct diurnal cycle of NO_x that has been
12 attributed to boundary layer stability and the flux of NO_x released from the snowpack both
13 driven by diel changes in solar radiation (France et al., 2011). The second study was dedicated
14 to the measurements of concentrations of HONO during the summer 2010/2011 (Kerbrat et
15 al., 2012) with a LOPAP technique. Kerbrat et al. (2012) concluded that the observed large
16 mixing ratio (~30 pptv) of HONO would require an unexpectedly large photochemical source
17 of HONO from the snowpack, if the measurements of gas-phase HONO were not biased due
18 to an unknown interference.

19 In the framework of the OPALE project aimed at characterisation of the oxidative
20 capacity of the atmosphere in the region of East Antarctica (Preunkert et al., 2012) a field
21 campaign was carried out at the top of the high Antarctic Plateau, at Concordia station, from
22 December 2011 to January 2012. The first results of this campaign are presented in several
23 publications accompanying this article, including (Frey et al., this issue) for NO and NO₂,
24 (Legrand et al., this issue) for HONO, and (Preunkert et al., this issue) for HCHO. Here
25 presented for the first time are measurements of concentrations of OH and RO₂ radicals
26 conducted on the East Antarctic Plateau at the Concordia station (Dome C). Sources and sinks
27 of these radicals are discussed in the light of concurrent chemical observations made during
28 the campaign, including HONO, NO, NO₂, H₂O₂, HCHO, and O₃, as well as surface
29 meteorological parameters, physics of the boundary layer and photolysis rates.

2. Methods

Measurements of atmospheric concentration of OH and RO₂ (the sum of hydroperoxy HO₂ and organic peroxy radicals) radicals were conducted from 19 December 2011 to 9 January 2012 at Concordia station (Dome C, 75.10° S, 123.31° E, altitude 3233 m).

The weather at Concordia is dominated by weak katabatic winds ($\sim 3 \text{ m s}^{-1}$) and clear sky conditions with frequent presence of elevated cirrus clouds. Daylight lasts 24 h with a significant diurnal variation of solar radiation (as shown in Figures 1a and 1b for the photolysis rate coefficients for NO₂ and O₃) resulting in a strong diurnal cycle in near-surface temperature (Figure 1c) and wind speed. During the OPALE campaign the median values of the temperature at height of 1m and the wind speed ranged from -36°C and 2 m s^{-1} at 03:00 (all times are local times equivalent to UTC+8 h.) to -27°C and 4 m s^{-1} at 15:00, respectively. The diurnal solar cycle is responsible for a well defined diurnal cycle of boundary layer structure (Figure 1c). Starting from about 7:00 in the morning the diurnal heating and upward sensible heat flux (King et al., 2006) drive formation of the convective mixing layer reaching a maximum height of 300-600 m at about 17:00. During the night the boundary layer is stably stratified and confined to a height of several meters. The boundary layer height presented in Figure 1c comes from the Modèle Atmosphérique Régional (MAR) (Gallée et al., this issue) briefly described in Section 2.3.

The measurement site was located in a designated clean-air sector 0.7 km to the south of the main station buildings. During the measurement period the wind direction was predominantly from the south, median value of 180° , with few pollution events (on 19-Dec, 31-Dec and 1-Jan) due to the wind coming from the station, wind sector of $10 - 50^{\circ}$ (Figure 1c). The data corresponding to the pollution events were filtered out.

2.1 Radical measurements

Concentrations of OH and RO₂ radicals, as well as sulfuric acid (not shown here), were measured using chemical ionisation mass spectrometry (CIMS) (Eisele and Tanner, 1991; Berresheim et al., 2000). Detailed description of the instrument is presented elsewhere (Kukui et al., 2008; Kukui et al., 2012; Michoud et al., 2012). Here we briefly present the principle of the method and report details about the setup of the device and working conditions applied during measurements at Dome C.

1 The concentration of OH radical was measured by titrating atmospherically sampled
2 OH radicals with SO₂ to form H₂SO₄ in a chemical conversion reactor in the presence of
3 water vapor and oxygen [Eisele and Tanner, 1991; Tanner et al., 1997; Berresheim et al.,
4 2000]. H₂SO₄ was detected by mass spectrometry as the HSO₄⁻ ion. The HSO₄⁻ ion was
5 produced by chemical ionisation with NO₃⁻ in an ion-molecule reactor following the
6 chemical conversion reactor. To distinguish for atmospheric sulfuric acid the chemical
7 titration was performed using isotopically labelled ³⁴SO₂ leading to the formation of H₂³⁴SO₄.
8 The concentration of total peroxy radicals RO₂ was measured by converting RO₂ into OH
9 radicals via reactions with NO injected in the chemical conversion reactor [Reiner et al.,
10 1997] followed by conversion of OH into sulfuric acid.

11 During measurements at Dome C and similarly to previous measurements in Coastal
12 Antarctica at Dumont d'Urville (DDU) (Kukui et al., 2012) the instrument was installed in a
13 shipping container with the chemical conversion reactor fixed to the roof of the container via
14 an interface cap covered with a PTFE sheet. The sampling aperture of the reactor (3 mm
15 diameter) was positioned 50 cm above the roof and about 3 m above the snow surface.

16 Ambient air was sampled at a volumetric flow rate of 7.4 standard litres (sl) min⁻¹
17 creating turbulent flow in the chemical conversion region of the reactor (Reynolds Number
18 $Re = 6400$). The turbulent flow conditions minimize possible influence of wind speed on the
19 measurements and ensure fast mixing of reactants. The reactants used for the chemical
20 conversion (³⁴SO₂ and NO) and the radical quencher (NO₂) are introduced into the reactor
21 through a set of injectors. NO₂ used as a scavenger removes not only the OH radicals, but also
22 peroxy radicals converting them into HO₂NO₂ and RO₂NO₂ nitrates. The input flow rates of
23 the reactants were similar to those previously used with this instrument (e.g. Kukui et al.,
24 2012), while the sampling flow rate was a factor of 2 smaller than usual. These flow rates
25 were necessary to compensate for the reduced pressure at Dome C (620 hPa) compared to sea-
26 level operation of the instrument, and provided comparable reaction times to previous
27 deployments of this instrument. Switching the reactant flows between the different injectors
28 allows measurements in four different modes: the background mode, two different OH radical
29 measurement modes and the RO₂ radical measurement mode. The two OH measurement
30 modes differ by the time used for the chemical conversion, 4 and 20 ms (Kukui et al., 2008;
31 Kukui et al., 2012). Ratio of the signals with the short and the long conversion times may be
32 used as an indicator of an artificial OH formation in the reactor [Kukui et al., 2008].

Measurements of OH, RO₂ and H₂SO₄ were performed by monitoring the peak intensities at m/z=62 (NO₃⁻), m/z=99 (H³⁴SO₄⁻) and m/z=97 (H³²SO₄⁻). The detection of H³⁴SO₄⁻ and H³²SO₄⁻ corresponds to the measurement of the radicals (OH or RO₂) and H₂SO₄, respectively. The ion peak intensities were measured sequentially resulting in nine measurements of OH and one measurement of RO₂ for every 28 minutes. Every measurement of OH was derived from 1 min of OH ion signal count and two 30 s background ion signal counts before and after the OH signal measurement. RO₂ was measured at the end of the OH detection sequence by switching on the NO flow to the corresponding injector for the duration of 2 min. To avoid any possible influence of traces of NO on the OH measurements a time delay of 10 min was introduced after switching off the NO flow and before starting the next OH measurement sequence to ensure flushing of the chemical conversion reactor. The measurements of OH and RO₂ radicals were averaged to 15 minute and 30 minute time intervals, respectively.

The concentration of the radicals, [R], is derived from the measured ratio of the H³⁴SO₄⁻ and NO₃⁻ ion peak intensities, I₉₉/I₆₂: $[R] = C_R \times \ln(1 + I_{99} / I_{62})$, where C_R is a calibration coefficient determined in calibration measurements by production of a known concentration of OH or RO₂ radicals in a turbulent flow reactor by photolysis of water vapor at 184.9 nm (Heard and Pilling, 2003, and references therein; Faloona et al., 2004; Dusanter et al., 2008). Except for additional thermo-stabilisation of a Pen-Ray mercury lamp and a VUV phototube the construction of the calibration cell was the same as previously described in Kukui et al., (2008). The concentration of OH and HO₂ radicals generated in the turbulent flow was calculated from the monitored photon flux and H₂O concentration. For precise control of the concentrations of H₂O at low temperatures the gas manipulation system for the introduction of the mixture of pure air and water vapor into the photolysis reactor was modified by replacing the previously used water trap by a liquid flow controller (Bronkhorst, μ-FLOW series L01, 1.4 g/h) allowing simulation of typical atmospheric humidities encountered at Dome C (e.g., 50-70% at -30°C). During the calibrations at Dome C the previously employed cooled mirror dew-point transmitter used for the humidity measurements in the photolysis reactor was found to be unreliable at low temperatures and was replaced by a capacitive humidity sensor (Vaisala, HMP155) providing more accurate humidity data. The water vapor/air mixture was generated inside the container and introduced to the calibration cell positioned on the roof of the container through a 10m Teflon tube placed outside of the container, providing the cooling of the calibration gas mixture to the

1 ambient temperature. Despite these modifications frequent difficulties were encountered
2 maintaining stable humidity under conditions of low temperatures at Dome C, limiting
3 calibration accuracy.

4 The atmospheric concentration of total peroxy radicals RO_2 was measured assuming
5 that the HO_2 and CH_3O_2 radicals represent the major part of all RO_2 radicals at Dome C, i.e.
6 $[\text{RO}_2] = [\text{HO}_2] + [\text{CH}_3\text{O}_2]$, with a ratio of $[\text{HO}_2]/[\text{RO}_2]$ of about 0.7, as informed from the
7 model calculations (see below). The calibration of HO_2 and CH_3O_2 was performed by adding
8 into the calibration cell photolysis reactor either CO or CH_4 converting any OH radical to
9 HO_2 or CH_3O_2 , respectively [Hanke et al., 2002; Fuchs et al., 2008]. The sensitivity to HO_2
10 was found to be $(15 \pm 2)\%$ higher than that for the CH_3O_2 .

11 The overall accuracy of the calibration coefficients was estimated taking into account
12 uncertainties of all parameters used for calculation of the radical concentrations in the
13 photolysis reactor and the precision of the measurements of the ratio I_{99}/I_{62} . The main sources
14 of the calibration uncertainty at Dome C were the estimation of the photon flux ($\pm 15\%$) and
15 the uncertainty of the measurement of humidity ($\pm 30\%$). The overall estimated calibration
16 accuracy (2σ) was of 36% for OH and of 40% for HO_2 . The uncertainty of the measurements
17 of RO_2 , accounting for possible variation of the RO_2 composition, was estimated to be of 45%
18 at Dome C. Accounting for the calibration uncertainties and measurement precision, the
19 overall 2σ uncertainty of the 15 min averaged measurements of OH and RO_2 was estimated to
20 be 40% and 47% during the day time and 60% and 50% during the night time, respectively.
21 The lower limits of detection for OH and RO_2 radicals at signal-to-noise ratio of 3 and a 2
22 minute integration time were 5×10^5 molecule cm^{-3} and 2×10^6 molecule cm^{-3} , respectively.

23 To avoid possible contamination of ambient air by the SO_2 , NO and NO_2 reactants
24 added to the chemical conversion reactor, a trap was set up at the pumps exhaust by using two
25 100 L cylinders containing zeolites. The cylinders were refilled several times during
26 measurements. Flexible exhaust tube of 30 m length was always placed downwind from the
27 container. When the exhaust tube was intentionally placed upwind and close to the radicals
28 sampling point no effect on radical measurements was detected. Also, no influence of the
29 exhaust on the measurements of NO_x and HONO could be noticed.

2.2 Other measurements

Other chemical measurements conducted at Dome C during the campaign that are relevant to the discussion of sources and sinks of OH and RO₂ radicals include O₃, HCHO, H₂O₂, HONO, NO, NO₂ and photolysis coefficient values. Their mean values and ranges are summarised in Table 1, while the detailed discussion of these data and description of the instruments and applied working conditions during the campaign are presented in the corresponding companion papers.

Surface ozone was monitored by UV absorption (Thermo electron Corporation model 49I) deployed at Dome C since 2007 (Legrand et al., 2009). Atmospheric HCHO measurements were performed with a fluorimetric method using commercial Aerolaser analyzer (model AL-4021) (Preunkert et al., 2014, and this issue). A fluorimetric two-channel technique was applied for determinations of H₂O₂ (Aerolaser, Model AL2021)(Preunkert et al., 2012).

NO_x was measured with a 2-channel chemiluminescence detector with one channel used for NO detection and the other for the sum of NO and NO originating from the quantitative photolytic conversion of NO₂ (Bauguitte et al., 2012; Frey et al., 2013, and this issue). The NO₂ and NO measurements are discussed in Frey et al. (this issue). The ratios of NO₂ to NO observed at Dome C during 2011-2012 campaign were up to 3 times larger than in 2009-2010 (Frey et al., 2013) and significantly larger, up to 7 times, than the ratios estimated assuming photochemical steady-state (PSS) conditions for NO_x. It is suggested that some part of this inconsistency may be due to unknown interference leading to an overestimation of the NO₂ concentrations (Frey et al., this issue).

The photolysis rate constants, J, were calculated from measurements of “actinic flux” (Madronich 1987) measured by a Met-Con 2π spectral radiometer with a CCD detector and a spectral range from 285 to 700 nm. The Met-Con Spectral radiometer was calibrated before and after the campaign using a NIST traceable standard 1000 W tungsten halogen lamp. No significant changes were observed in the performance of the spectral radiometer. The spectral radiometer was mounted on a mast of 1m height on the roof of the container used for the radical measurements. A shadow band was fitted to provide a horizontal horizon. Downwelling unweighted radiance over a complete hemisphere, was recorded as a 5 second average for each of the 532 pixels and internally interpolated to a 1nm resolution over 285-700 nm. The atmospheric photolysis coefficients, J, were calculated using the measured

actinic flux along with quantum yields and absorption cross-sections from Sander et al., (2011). The principle of using a 2π CCD Met-Con spectral radiometer to accurately determine photodissociation rate constants, J , has been previously demonstrated by Jäkel et al., (2007). Total 4π steradian radiance was calculated by multiplying the downwelling 2π steradian radiance by a value of 1.9. The value of 1.9 is based on measurements of downwelling and upwelling radiance by inverting the spectral radiometer.

HONO was measured with a long path absorption photometry (LOPAP) ((Heland et al., 2001; Kleffmann et al., 2002) at height of 1m above the snow surface. In spite of the use of the LOPAP, thought to be free of measurement artefacts, mixing ratios of HONO observed at Dome C in December 2011/January 2012 (hourly means of 35 ± 5 pptv, Legrand et al., this issue) are in the same range as previously observed in December 2010/January 2011 (hourly means of 30.4 ± 3.5 pptv) by Kerbrat et al. (2012). As discussed by Legrand et al. (this issue), laboratory experiments with irradiated surface snows collected at Concordia reveal that the snowpack may be a very significant source of HONO. It is shown that this source only accounts for a third of observed HONO mixing levels at 1 m height at Concordia. Legrand et al. (this issue) report tests done both in the field and in the lab that tend to suggest an overestimation of HONO measurements in the range of 10 to 20 pptv due to the presence of HO_2NO_2 in the range of 50-100 pptv in the cold atmosphere at Dome C.. This range of HO_2NO_2 mixing ratios is in agreement with the median $[\text{HO}_2\text{NO}_2]$ of 80 pptv estimated from RO_2 and NO_2 levels measured at Dome C (see Section 3.2). Also, as discussed by Legrand et al. (this issue), similar levels of HO_2NO_2 were previously observed in Antarctica.

2.3 Model calculations

Observed concentrations of OH and RO_2 were compared with those calculated using a 0D box model. Photostationary concentrations of OH and RO_2 were calculated by performing numerical integration using a subset from the Master Chemical Mechanism, MCM v3.2 (Jenkin et al., 1997; Saunders et al., 2003) (website: <http://mcm.leeds.ac.uk/MCM>). The subset includes 159 reactions comprising the MCM inorganic section, photochemistry, loss of HNO_3 and RO_2NO_2 by dry deposition and methane chemistry extended with CH_3CHO and CH_3COCH_3 . The model ran using the MATLAB package for the entire period from 19th December to 10th January with 15 min time step and initiated by three-day spin-up for the first day. The calculations were constrained by the 15 min averaged measurements of HONO, NO , NO_2 , O_3 , HCHO, H_2O_2 , photolysis coefficients and meteorological parameters. Concentration

1 levels of CO, CH₄, H₂, CH₃CHO, CH₃OOH, CH₃COCH₃ and CH₃COOH, were estimated as
2 described in Section 3.2.

3 The vertical distribution of HONO in the boundary layer was modelled using a 1D
4 chemistry-transport box model with a vertical distribution of turbulent diffusivity and
5 boundary layer heights calculated by the regional atmospheric MAR model (Modèle
6 Atmosphérique Régional). A detailed description of the model and its validation with respect
7 to observations from the Automatic Weather Station at Dome C is given in Gallée and
8 Gorodetskaya (2008), Gallée et al., (this issue) and references therein. The turbulence scheme
9 is based on an E-e scheme and on the Monin-Obukhov Similarity theory (MOST), outside and
10 inside the lowest model layer of MAR, respectively. Similar to calculations performed by
11 Legrand et al., (this issue), we used the MAR data obtained with a horizontal resolution of 20
12 km centred at Dome C; a vertical resolution of 0.9 m up to a height of 23 m above the surface
13 increasing upward to about 50 m at the height of 500 m; 100 vertical levels with a top level at
14 1 hPa. For the 1D box model calculations the values of the vertical diffusivity, K_z, were
15 linearly interpolated to the vertical grid of 0.1 m from the surface to 5 m, 0.2 m from 5 to 7 m,
16 0.5 m from 7 to 10 m, around 1 m from 10 to 20 m and then increases up to 120 m at 1200 m
17 height (the BL upper bound was always lower than 1200 m during the OPALE campaign).
18 The boundary layer height is defined by MAR as the height where the turbulent kinetic
19 energy decreases below 5 % of the value at the lowest layer of the model. The calculated
20 boundary layer height profile, as well as measured temperature and wind direction profiles are
21 presented in Figure 1.

22 23 **3. Results and Discussion**

24 **3.1 Presentation of the measurements of OH and RO₂ radicals**

25 Measurements of the concentration of OH and RO₂ radicals are presented in Figures 1
26 and 2. The radical concentrations exhibited clear diurnal profiles driven by the solar radiation
27 cycle and ranged from 3×10^5 to 7.5×10^6 and from 1×10^7 to 2×10^8 for OH and RO₂,
28 respectively, in units of molecule cm⁻³. As shown in Figure 2, the diurnal profiles of OH and
29 RO₂ radicals follow the diurnal variation NO₂ photolysis coefficient, J(NO₂). At the same
30 time, one can notice some deviation of the diurnal concentration profiles of OH and RO₂ from
31 the J(NO₂) profile with larger concentrations for OH and lower for RO₂ in the afternoon. This

1 is reflected in the diurnal profile of the ratio of [OH] to [RO₂] (Figure 2c) which shows a
2 diurnal profile with lower values of [OH]/[RO₂] during the day and factor of ~2 larger in the
3 afternoon. Notably, the [OH]/[RO₂] diurnal profile correlates with the daily profile of the
4 concentration of NO (Figure 2c).

5 The median concentrations of RO₂ and OH radicals measured at Dome C are compared
6 to those observed at the South Pole in Table 1. At Dome C the J(O(¹D)) daily median values
7 at 5:00 and 19:00 ($9 \times 10^{-6} \text{ s}^{-1}$) are similar to median J(O(¹D)) observed at the SP ((8.5-
8 $9.0) \times 10^{-6} \text{ s}^{-1}$). Comparing the corresponding concentrations of OH radical one can see that the
9 median values at Dome C are close to that observed at the SP for 5:00 and somewhat higher at
10 19:00, 2.5×10^6 and 3.8×10^6 , respectively, compared to 2.3×10^6 at the SP during ISCAT 2000.
11 The concentrations of NO at the SP were similar to the observed at Dome C, 88 pptv and 77
12 pptv, respectively.

13 As seen in Figure 3, the concentrations of both OH and RO₂ correlate linearly with
14 J(NO₂) with about 60% and 80% of the variability of OH and RO₂, respectively, explained by
15 the variability of J(NO₂). The relationship of [OH] with J(O(¹D)) was close to a power-law
16 dependence with an exponent of ~0.5 in accordance with a typical close to quadratic
17 dependence of J(O(¹D)) on J(NO₂) observed at Dome C. As seen from the color coding in
18 Figure 3 by concentration of NO of the graph points, there is an obvious correlation with
19 [NO], positive for [OH] and negative for [RO₂]. In fact, about 80% of the [OH]/[RO₂]
20 variability may be explained by the linear correlation with [NO] (Figure 3c).

21 The important role of NO in controlling the concentrations of OH and RO₂ is seen on
22 Figure 4 where [OH] and [RO₂] are normalised by J(NO₂) to remove the dependence on solar
23 radiation and plotted against [NO]. For concentrations of NO of up to ~150 pptv the
24 concentration of OH rises and then level off, while [RO₂] exhibits the reverse dependence on
25 [NO]. These dependences are very similar to those observed at the SP (Figures 2 and 7 in
26 Mauldin et al., 2004) and can be explained in a similar way: when the concentration of NO is
27 small, the concentration of OH increases due to the enhanced recycling from RO₂ until the
28 losses of RO₂ and OH in reactions with NO₂ become important compared to other loss
29 processes and therefore compensate the enhanced OH formation (see below for further
30 discussion).

31 Owing to an approximate linear correlation of [HONO] with [NO] observed at Dome C
32 (Legrand et al., this issue) together with a approximately linear relation between J(HONO)

and $J(\text{NO}_2)$ the dependence of the concentrations of OH and RO_2 on $J(\text{HONO})$ and HONO is very similar to that on $J(\text{NO}_2)$ and $[\text{NO}]$ presented in Figures 3 and 4, implying the concentration of HONO also could be an important parameter controlling the radical variability.

3.2 Radical sources and sinks

The sources and sinks of OH and RO_2 radicals at Dome C were calculated using the radical field measurements and other available relevant observations presented in Table 1. Some of the key species involved in the radical production and losses, namely CO, CH_4 and H_2 , were not measured. For CO, a mixing ratio of 40 ± 4 ppbv was assumed referring to the value observed at the South Pole (Novelli and Masarie, 2013). Similar mixing ratios of CO for the period of December - January have been measured during ISCAT 2000 at the SP (Davis et al., 2004), at DDU (Preunkert et al., 2012). For methane and H_2 mixing ratios the values of 1.8 ppmv (Steele et al., 2002) and 520 ppbv (Steele et al., 2003) are adopted, respectively, based on measurements made at other Antarctic sites.

Measurements of acetaldehyde are sparse in Antarctic regions. As discussed by Legrand et al. (2012), at the coastal site of DDU an acetaldehyde background mixing ratio close to 80 pptv can be assumed, though this value may be highly variable over the Southern ocean (5 to 50 pptv). Hamer et al., (2007) reported a mixing ratio of CH_3CHO of 60 pptv at the SP. In our calculations we used a value of 60 pptv with an uncertainty of 20%. Methyl hydroperoxide (CH_3OOH), acetic acid (CH_3COOH) and acetone (CH_3COCH_3) were also considered in our calculations. CH_3OOH was estimated from observations of H_2O_2 made at Dome C (mean value of 166 pptv, see Table 1) and assuming that it represents 40 ± 10 % of H_2O_2 as reported by Frey et al. (2005] at the SP. For CH_3COCH_3 a typical mixing ratio of 130 ± 30 pptv was used on the basis of observations made at the SP (Hamer et al., 2007). For CH_3COOH , Legrand et al. (2012) measured 60-70 pptv at Dome C between November and February.

The calculated rates of radical sources and sinks are presented in Figures 5 and Table 2. Based on available measurements the major primary radical source is the photolysis of HONO (1), with other net sources, namely, photolysis of HCHO (7), H_2O_2 (2), O_3 (3) and CH_3CHO (8) being less important and contributing altogether less than 30% of the net radical production (the numbering of the reactions is according to the Table 2). It is important to

emphasize here that, as detailed in section 2.2, the HONO data used in these calculations are thought to be biased by the presence of HO₂NO₂ (Legrand et al., this issue). Since the raw HONO concentration data cannot be accurately corrected for this measurement artefact, we consider in the following discussion (Section 3.4 and 3.5) several scenarios for HONO mixing ratios.

The recycling of OH and RO₂ radicals proceeds mainly via the reactions of HO₂ with NO (5) and of OH with CO (10) and CH₄ (11), with the production rate of OH from HO₂+NO being about half of the generation rate of OH via the photolysis of HONO. Although being less important, additional regeneration of RO₂ by the reactions of OH with HCHO, CH₃CHO, O₃ and H₂ (12-15) remain significant.

Net loss of the radicals proceeds mainly via the reactions OH+NO₂ (18), RO₂+NO₂ (24) and radical cross reactions OH+RO₂ (20) and RO₂ +RO₂ (25). Note that radical cross reactions become particularly important during the day when concentration of RO₂ is large (Table 2). Reactions of OH with NO, HONO, RO₂NO₂ and HNO₃ contribute together about 16% to the radical net losses. The contribution of the reaction of HO₂(H₂O) with NO₂ (Li et al., 2014) to the RO₂ losses is estimated with the rate constants given in Legrand et al. (this issue) to be less than 1%.

As the losses of OH and RO₂ via the reactions with NO₂ may be overestimated due to unknown interference in the NO₂ measurements (Frey et al., this issue) we also present in the Table 2 (values in parenthesis) the radical losses for [NO₂] estimated assuming PSS conditions for NO_x. In this case the net daytime radical losses are dominated by the radical cross reactions RO₂+RO₂ (25) and OH+RO₂ (20).

According to the above mechanism derived from the field observations, the sum of peroxy radicals RO₂ is composed predominantly of HO₂ and CH₃O₂, [RO₂] = [HO₂] + [CH₃O₂]. The ratio of [HO₂] to [RO₂] which was required for calculating the radical sources/sinks was estimated using steady-state calculations accounting for all identified sources and sinks of HO₂ and CH₃O₂. The resulting value of [HO₂]/[RO₂] is 0.67±0.05(1σ) and is close to the ratio of 0.73 estimated by only accounting for the production of RO₂ in the reactions of OH radical with CO and CH₄ and the loss of RO₂ via reactions of RO₂ with NO.

Concentrations of peroxy nitrates (CH₃O₂NO₂ and HO₂NO₂) involved in radical loss reactions (see Table 2) were not measured at Dome C but were estimated assuming steady-state conditions and accounting for their losses via photolysis, the reaction with OH, thermal

decomposition and a surface deposition of $7 \times 10^{-5} \text{ s}^{-1}$ (Slusher et al., 2002). The calculated mixing ratios of HO_2NO_2 and $\text{CH}_3\text{O}_2\text{NO}_2$ were ~ 80 pptv and ~ 20 pptv, respectively. These mixing ratios of HO_2NO_2 are somewhat higher than $[\text{HO}_2\text{NO}_2]$ of 40-60 pptv observed at the South Pole (Slusher et al., 2010) under conditions of significantly lower $[\text{NO}_2]$ (estimated at SP from NO observations assuming steady-state). Assuming the steady-state NO_2 concentrations at Dome C the estimated mixing ratios of HO_2NO_2 and $\text{CH}_3\text{O}_2\text{NO}_2$, are significantly lower: ~ 10 pptv and ~ 3 pptv, respectively. In the work presented here the calculated steady-state concentrations of peroxy nitrates were used to estimate the effective loss rates of RO_2 radicals in the reactions with NO_2 by accounting for the regeneration of RO_2 via RO_2NO_2 thermal decomposition.

The mechanism presented above of the radical production and loss is supported by examination of specific correlations. The major sources of OH radical, both the photolysis of HONO and the recycling from HO_2 , are expected to correlate with photolysis rates. Hence, the observed close to linear correlation between $[\text{OH}]$ and $J(\text{NO}_2)$ or $J(\text{HONO})$ (Figures 3) tends to support the importance of these two mechanisms of the production of OH radical. However, the correlation of $[\text{OH}]$ with $J(\text{NO}_2)$ explains only about 60% of $[\text{OH}]$ variability, while an additional source of $[\text{OH}]$ variability may come from the variability of $[\text{HONO}]$ and/or $[\text{NO}]$ as it can be seen from Figure 3. To account for the variability of $[\text{HONO}]$ and $[\text{NO}]$, in Figure 6 we plotted $[\text{OH}]$ against production rates of OH radical via photolysis of HONO, (P_{HONO}), and via reaction of HO_2 with NO, ($P_{\text{HO}_2+\text{NO}}$). The variability of $P_{\text{HO}_2+\text{NO}}$ or P_{HONO} then explain $\sim 80\%$ of the variability of OH.

3.3 Photochemical budget of radicals

According to the calculated sinks of OH and RO_2 radicals their lifetimes were less than 3 s and 100 s, respectively. The time scales for the variability of atmospheric parameters at Dome C (boundary layer height and vertical diffusivity, solar radiation, NO_x concentration etc.) were typically significantly larger, more than 10 minutes. Hence, assuming validity of a steady state approximation for OH and RO_2 , their sources and sinks should be balanced. However, as shown in Figure 5 and Table 2, on the basis of observations the sum of the radical production rates exceeds by about (40-90)% and 25% the sum of loss rates for OH and RO_2 radicals, respectively. Considering the primary sources and net sinks of the sum of OH and peroxy radicals, the measured primary radical production is larger than their measured total removal rate by a factor of 2 and 3 for midnight and noon times, respectively.

A similar result of the budget analysis follows from the comparison of the net OH and RO₂ production rates, i.e. from the difference of the sum of their primary sources and the sum of their net removal, and the total rate of the radical recycling. Under steady state conditions the net production (or removal) rate of OH, $P_{pr}^{net}(OH)$, should be compensated by the net removal (or production) rate of RO₂, $-P_{pr}^{net}(RO_2)$, and equal to the net recycling rate of OH to RO₂ (or RO₂ to OH), $R^{net}(OH \rightarrow RO_2)$, (see Table 2):

$$P_{pr}^{net}(OH) = R^{net}(OH \rightarrow RO_2) = -P_{pr}^{net}(RO_2)$$

However, as seen in Table 2, according to the field measurements the net primary production rate of OH significantly exceeds both the OH to RO₂ recycling and the net RO₂ removal rates. At the same time, the net conversion rate of OH to RO₂ is not compensated by the measured net removal rate of RO₂. This interpretation shows in a different way the same result as the Figure 5: for both OH and RO₂ radicals the measured radical production rate exceeds their loss rate, although for RO₂ the difference is less significant.

The observed misbalance between radical production and loss could result from underestimated or unaccounted radical losses, as well as from overestimated radical sources. As the main radical loss processes identified at Dome C were the reactions of radicals with NO₂ and radical cross reactions the underestimation of the radical losses could be related to an underestimation of measured concentration of NO₂ and/or concentrations of OH and RO₂ radicals. The underestimation of the radical concentrations by a factor of 2 is well outside the estimated uncertainties for the measurements of OH and RO₂, although we can not completely exclude some unknown error in the radical calibration procedure.

Considering the possibility of the underestimation of the concentration of NO₂, sensitivity analysis shows that increasing of the concentrations of NO₂ by a factor of ~3 would result in a fair agreement of the model with the observations. However, as the observed [NO₂]/[NO] ratios at Dome C are already very high it is very unlikely that measured NO₂ was underestimated. As discussed in Frey et al., (2013, this issue) the ratios of [NO₂]/[NO] observed at Dome C are not consistent with other observations available at Dome C. Accounting for the photolysis of NO₂ and conversion of NO to NO₂ in the reactions with measured [RO₂] and [O₃] results in the ratio of [NO₂] to [NO] about a factor of 7 lower compared to the measured values suggesting that there is a missing mechanism of the conversion of NO to NO₂. An explanation evoking an underestimation of the measured RO₂ can be excluded, because the concentrations of RO₂ radicals needed to explain the observed

ratio of $[\text{NO}_2]/[\text{NO}]$ would be a factor of 20 larger than measured. Another possibility would be an additional conversion of NO to NO_2 in presence of halogens (i.g., ClO, BrO, IO) as was found at other polar sites, e.g. at the coastal site of Halley (Bauguitte et al., 2012). However, to explain the observed ratio of $[\text{NO}_2]/[\text{NO}]$ at Dome C very large concentration of halogen species would be required, about 60 pptv in case of BrO and even higher for ClO. Such a large halogen mixing ratio is contradicted by measurements of BrO at Dome C, i.e. Frey et al., (this issue) report the BL mixing ratios of BrO of ~ 2 pptv. Hence, we conclude that either there is some unknown mechanism of NO to NO_2 conversion, or there was some interference affecting the NO_x measurements.

The analysis performed here of the radical chemistry at Dome C could be affected in both cases: the missing NO_x chemistry could interfere with chemistry involving OH and RO_2 , i.e. by shifting the ratio $[\text{RO}_2]/[\text{OH}]$ towards OH, like in the case of efficient halogen chemistry at Summit, Greenland (Liao et al., 2011), while biased measurements of NO_x could affect the calculated radical losses and interconversion rates. Further speculations about possible impact of an unknown NO_x regulating mechanism on the OH and RO_2 chemistry are not feasible at this stage. Concerning possible interference in NO_x measurements, any correction consisting in a reduction of NO_2 would result in weaker radical losses and, hence, even larger overestimation of the radical sources. As shown in Table 2 the assumption of steady-state NO_2 concentrations lead to a significant overestimation of the net radical production for RO_2 and (RO_2+OH) even when neglecting net OH production by the photolysis of HONO. For OH budget, neglecting the net OH production by the HONO photolysis would lead to an underestimation of the OH production.

Considering the possibility of some overestimation of the OH radical production rate and independent of discussions carried out elsewhere (Legrand et al. this issue), one can see from the Figure 5 and Table 2 that among all the measured radical sources only the photolysis of HONO is large enough to explain, in case of its overestimation, the observed misbalance. In the following section we compare the observed concentrations of OH and RO_2 with model predictions to test the sensitivity of the modelled $[\text{OH}]$ and $[\text{RO}_2]$ to the concentration of HONO.

3.4 Comparison with 0-D model: sensitivity to HONO

The simulations of concentration profiles of OH and RO₂ were conducted with different constraints on the concentration of HONO: taken as measured by LOPAP, the LOPAP measurements reduced by factors 2, 4, and estimated accounting for HONO production in HO+NO and HONO removal by photolysis assuming PSS conditions. The modelled concentrations of OH and RO₂ radicals are presented in Figures 7 and 8. Accounting for all radical sources including the photolysis of HONO leads to about a factor of 2 overestimation for modelled [RO₂] and [OH] with moderate correlation of the calculated and observed concentrations of OH and RO₂ radicals. Assuming HONO at PSS leads to an underestimation of [OH] and [RO₂] with a ratio of modelled to observed concentrations (M/O) of about 0.5 and a distinct difference between modelled and observed diurnal profiles (Figure 8), with better agreement during the daytime. As shown in Figure 8 the M/O becomes closer to 1 by decreasing [HONO] from the measured to concentrations reduced by a factor of 4. Reducing the concentration of HONO by 0.25 gives the best agreement for OH, RO₂ and their ratio.

Similar to the approach adopted at the SP (e.g., Davis et al., 2004) we have tested the model assuming PSS HONO concentrations and using concentrations of NO₂ calculated by assuming photostationary ratio of [NO₂]/[NO] calculated from the observed concentrations of NO, O₃ and RO₂. In this case, similar to the SP results, we obtain quite a good description for [OH], although with up to a factor of 1.5 overestimation of [RO₂] and [RO₂]/[OH] ratio at noon (Figure 8).

Another insight on the relationship between the calculated concentrations of radicals and [HONO] can be gained by comparing the dependencies of observed and calculated [OH] and [RO₂] normalised by J(NO₂) on [NO] (Figure 4). The model clearly shows that neglecting HONO photolysis and using constraints by measured concentrations of NO_x leads to a clear disagreement with observations. In this case, the calculated roll-off of normalised [OH] starts at a mixing ratio of NO of about 50 pptv (Figures 4a) as a consequence of fast losses due to large [NO₂] and the lack of additional OH production at higher concentrations of NO_x. When it is assumed that measurements of HONO are correct, [OH] and [RO₂] are overestimated by a factor of almost two in the whole range of observed [NO]. A better description by the model is achieved either when reducing the HONO concentrations by a factor of 4 or by neglecting HONO and using [NO₂] calculated assuming PSS for NO_x (see also Figure 8). In the latter

case, the model underestimates the concentrations of radicals by 30-40% at large [NO], although the number of observations at large concentrations of NO (>200 pptv) is limited.

Considering diurnal profiles of the M/O ratio presented in Figure 8 one can see that although reducing the production rate of OH from the photolysis of HONO by reducing the concentration of HONO improves the agreement between the model and the observations, the diurnal profiles of the M/O ratio become more distinct indicating that a simple reduction of [HONO] cannot provide a satisfactory description for the diurnal concentration profiles of OH and RO₂. Thus, either some chemical mechanism is missing in the model and its effect on the M/O ratio becomes stronger at reduced rates of OH production or, the overestimation of the OH production rate is dependent on time of day (see discussion of effects related to BL diffusivity in Section 3.5). In fact, median values of the time-dependent correction of [HONO] necessary to provide agreement between calculated and observed radical concentrations can be estimated by solving radical sources and losses balance equations for the concentration of HONO. As shown in Figure 9, for the OH radical budget the balance is achieved by reducing P_{HONO} by a factor of three during the day with a smaller correction required during the night. Balancing the budget of primary production and net removal rates of radicals requires neglecting the photolysis of HONO during the day and reducing it to a quarter of its original value during the night time. According to a sensitivity analysis to different measured parameters the calculated to observed [HONO] ratios, [HONO]_{calc}/[HONO]_{obs}, are most sensitive to the concentrations of NO₂ and OH, RO₂ radicals. By assuming the PSS derived NO₂ concentrations, the balance for the OH radical budget is achieved by reducing P_{HONO} by a factor of 5, while for RO₂ and the sum of RO₂ and OH the radical production is overestimated even if the net source from HONO photolysis is neglected.

3.5 Comparison with 1D model

It follows from the analysis presented above in Section 3.4 that the concentrations of HONO observed at Dome C were probably too large and not compatible with the measurements of OH and RO₂. Legrand et al. (this issue) give indications of possible interference from HO₂NO₂ leading to an overestimation of the concentrations of HONO using the LOPAP technique. According to Legrand et al. (this issue), about 100 pptv of HO₂NO₂ may result in interference equivalent to about 15 pptv of HONO. As the interference has not

1 yet been well characterized and, in addition, no measurements of HO₂NO₂ were available at
2 Dome C, a correction of HONO data at Dome C is not presently possible.

3 As an alternative approach, we have compared the concentrations of HONO derived
4 by examining the radical budget (Figure 9) with the calculations assuming HONO snow
5 emissions at Dome C estimated from the laboratory studies of Legrand et al. (this issue). By
6 irradiating the surface of snow collected at Concordia and simultaneously measuring the
7 concentrations of HONO and NO_x produced from the snow the authors found that HONO
8 mixing ratios in the experiment chamber outflow were roughly 30-50% of the mixing ratio of
9 NO_x, depending on snow temperature. Under temperature conditions encountered at Dome C
10 the HONO/NO_x ratio ranged from 0.57 during the day (at -25°C) and 0.3 at night (at -35°C).
11 Applying this ratio to the NO_x snow emission flux at Dome C, derived from the NO_x vertical
12 gradients measured during the OPAL campaign by Frey et al. (this issue), Legrand et al. (this
13 issue) estimated a HONO flux at Dome C ranging from 0.2×10^9 molecules cm⁻² s⁻¹ at night to
14 1.5×10^9 molecules cm⁻² s⁻¹ at noon. These fluxes of HONO were used in the work described
15 here to estimate the concentrations of HONO at different heights above the snow using the 1D
16 chemistry-transport box model (section 2.3) with turbulent vertical transport and a simplified
17 chemistry scheme including HONO production via the snow emissions only and HONO
18 removal via photolysis. Formation of HONO in the reaction OH+NO contributing less than
19 10% to the concentration of HONO resulting from the snow emissions was neglected in the
20 present 1D calculations. Another gas-phase source of HONO via reaction of HO₂(H₂O)
21 complex with NO₂ was recently proposed by Li et al. (2014). Owing to low temperatures at
22 Dome C the contribution of this source to [HONO] is estimated to be less than 2-3% (Legrand
23 et al., this issue) and it was also neglected in the 1D model.

24 The results of the 1D calculations are shown in Figure 10 where the median diurnal
25 profiles of emission fluxes, boundary layer heights and simulated mixing ratios of HONO at
26 1m and 3m are shown for the period from 19th December to 5th January. Figure 10 shows that
27 the difference of HONO mixing ratios at 1m and 3m does not exceed 30% and, hence, the
28 vertical gradient of [HONO] and measurements of [OH] and [HONO] at different heights, 1m
29 and 3m, respectively, can only partly explain the overestimation of OH production from
30 HONO. This conclusion does not depend on the strength of HONO flux used in the model
31 because the relative difference between concentrations of HONO at different heights above

the snowpack is determined only by the diffusivity of the boundary layer and the lifetime of HONO.

The HONO mixing ratio-time profiles calculated with the 1D model are compared in Figure 10 with the HONO profiles resulting from analysis of the radical budgets. The levels of HONO derived from the OH budget with measured NO_2 are about 10 pptv higher than the HONO values obtained using PSS NO_2 concentrations. In both cases the HONO mixing ratios derived from the OH budget are in reasonable agreement with $[\text{HONO}]$ predicted by the 1D model (within 5 pptv). The 1D model reproduces also the diurnal HONO concentration profile with a minimum during the day and larger concentration of HONO in the evening resulting from interplay between emission rate and BL height variability (Legrand et al., 2013). For the concentrations of HONO derived from the OH+ RO_2 budget with measured NO_2 the model significantly underestimates the daytime $[\text{HONO}]$ but provides better agreement for the night and reproduces general temporal trend of HONO variability. The concentrations of HONO derived from the OH+ RO_2 budget with steady-state $[\text{NO}_2]$ are negative and not presented in Figure 10.

3.6 Ozone production

The RO_2 and NO measurements made at Dome C were used to estimate local boundary layer ozone production. As seen in Figure 11, the peak calculated ozone production rate ($\text{P}(\text{O}_3)$) is about 0.3 ppbv h^{-1} during daytime (using the measurements of RO_2 at 3 m, NO at 4 m above the snowpack and assuming $\text{P}(\text{O}_3)$ equal to NO_2 production rate in the reaction of RO_2 with NO). The production rate is in fairly good agreement with the previous estimation of 0.2 ppbv h^{-1} derived from examination of diurnal changes in the concentration of ozone (Legrand et al., 2009). The integrated 24h production of ozone reaches 4.7 ppbv d^{-1} at Dome C and is similar to the one calculated for the SP where the daily production of ozone was estimated from a model using measured concentrations of NO and OH to be of 2.2-3.6 ppbv d^{-1} for ISCAT 1998 (Crawford et al., 2001) and 3.2-4.8 ppbv d^{-1} for ISCAT 2000 (Chen et al., 2004).

It has to be emphasized with respect to the previous discussion of the ratio $[\text{NO}_2]/[\text{NO}]$ observed at Dome C that if the concentration of RO_2 radical was as large as needed to explain the observed $[\text{NO}_2]/[\text{NO}]$ ratio, the corresponding production rate of ozone would be as large

as 100 ppbv d⁻¹ and would strongly conflict with observed diurnal change of ozone (see Figure 3 in Legrand et al. (this issue).

4. Conclusions

Concentrations of hydroxyl radicals and the sum of peroxy radicals, RO₂, have been measured for the first time on the East Antarctic Plateau at the Concordia station (Dome C). The concentrations of OH and RO₂ radicals were found to be comparable to those observed previously at the South Pole (Mauldin et al., 2001, 2004, 2010) confirming that the elevated oxidative capacity found at the SP is not unique but a common characteristic of near-surface atmospheric layer for a large part of the high Antarctic plateau.

Similar to the findings at the SP the major explanation for the large concentrations of OH radical at Dome C was found to be the large concentrations of NO (Frey et al., 2013, Frey et al., this issue) leading to fast recycling of peroxy radicals to OH radicals. Also, similarly to the SP, the variability of the concentration of NO_x plays a major role in controlling the variability of radicals (OH and RO₂) at Dome C. In contrast to the SP, where there is no diurnal variation of solar radiation, and where radical levels are controlled by the concentrations of NO mostly via changing boundary layer properties (Neff et al., 2008), [OH] and [RO₂] at Dome C show strong diurnal variability correlating with the solar cycle, which in turn controls the rate of radical production and the rate of interconversion of OH and RO₂ radicals.

The large concentrations of radicals and NO result in ozone production in the BL at Dome C with a production rate of 0.1-0.3 ppb h⁻¹, similar to that observed at the SP.

The major primary sources of radicals in the atmosphere at Dome C are represented by the photolysis of HONO, HCHO, CH₃CHO and H₂O₂, (in order of decreasing significance), with photolysis of HONO deduced from measurements of HONO contributing for about 75% of total primary production of radicals. The main net losses of radicals are represented by their reactions with NO₂ and cross radical reactions. However, it is found, that these results are inconsistent with observations of radicals leading to about a factor of 2 overestimation of the concentrations of RO₂ and OH radicals. At the same time, neglecting the production of OH radical from the photolysis of HONO results in about a factor of 2 underestimation of the measured concentrations of radicals. Based on 0D modelling, to explain the observations of

OH and RO₂ radicals in this case an additional source of OH equivalent to about 25% of measured photolysis of HONO is required. Similar result follows from analysis of the photochemical budget of the OH radicals for which the balance is achieved by reducing P_{HONO} by a factor of three.

The conclusions based on the radical budget analysis and 0D modelling using the measured concentrations of NO and NO₂ may be significantly biased because the chemical mechanism derived from the available field observations at Dome C is inconsistent with observed large ratios of [NO₂] to [NO]. Assuming that measured NO₂ mixing ratios were overestimated due to unknown interference and using instead [NO₂] estimated assuming steady-state results in lower radical losses and, hence, stronger overestimation of the radical production. In this case, based on the analysis of the radical budgets the observed concentrations of OH radicals are consistent with the levels of HONO corresponding to about (15-20)% of the measured values, while for the sum of the radicals the radical production is overestimated even neglecting the net OH source from the photolysis of HONO. Based on 0D modelling steady-state derived NO₂, the measured OH concentrations are in agreement with steady-state HONO mixing ratios (about 1-2 pptv), while the concentrations of RO₂ radicals are overestimated by about 50% even neglecting the net radical production by the photolysis of HONO.

Hence, in both cases corresponding to the measured or the PSS derived concentrations of NO₂ the calculations, 0D modelling or budget analysis, overestimate the OH and RO₂ concentrations. If this inconsistency is due to an overestimation of the concentrations of HONO, the degree of the overestimation depends on the concentrations of NO₂ used in the calculations. Using the measured NO₂ results in an overestimation of HONO by a factor of 3-4. If the concentrations of NO₂ are estimated assuming steady-state conditions the net radical production from the HONO photolysis should be reduced by a factor of 5 or completely neglected based on the budget of OH or 0D modelling, respectively.

Assuming that HONO at Dome C originates from snow emissions with the emission strength evaluated by Legrand et al., (this issue) we obtain from a 1D model the concentrations of HONO corresponding to about 20-30% of measured [HONO] and the diurnal concentration profiles of HONO consistent with those calculated from the budget analysis of OH radicals with the concentrations of NO₂ either calculated assuming PSS or taken from the measurements. We suggest that an explanation for the overestimation of radical production could be an overestimation of measured concentration of HONO, which

1 may originate from the measurement interference from HO_2NO_2 affecting measurements of
2 HONO by LOPAP (Legrand et al., this issue). Even with a factor of 4 reduction in the
3 concentrations of HONO, the photolysis of HONO represents the major primary radical
4 source at Dome C accounting for about 45% of primary radical production.

5 Considering the observed uncertainties in HONO and NO_x measurements we suggest
6 that further studies of NO_x , HONO, peroxy nitrates (RO_2NO_2) and radical chemistry at
7 Antarctic Plateau are required with specific efforts dedicated to increase the reliability of
8 measurements (especially HONO and NO_2) under polar conditions.

9 10 **Acknowledgements.**

11 The OPALE project was funded by the ANR (Agence National de Recherche) contract ANR-
12 09-BLAN-0226. National financial support and field logistic supplies for the summer
13 campaign were provided by Institut Polaire Français-Paul Emile Victor (IPEV) within
14 programs N° 414 and 903. M.D. King and J.L. France wish to thank NERC (NE/F0004796/1
15 & NE/F0104788) and NERC FSF (555.0608 & 584.0609)

1 **References**

- 2 Bauguitte, S. J. B., Bloss, W. J., Evans, M. J., Salmon, R. A., Anderson, P. S., Jones, A. E.,
3 Lee, J. D., Saiz-Lopez, A., Roscoe, H. K., Wolff, E. W., and Plane, J. M. C.: Summertime
4 NO_x measurements during the CHABLIS campaign: can source and sink estimates unravel
5 observed diurnal cycles?, *Atmos. Chem. Phys.*, 12, 989-1002, 2012.
- 6 Berresheim, H., Elste, T., Plass-Dulmer, C., Eisele, F. L., and Tanner, D. J.: Chemical
7 ionization mass spectrometer for long-term measurements of atmospheric OH and H₂SO₄,
8 *Int. J. Mass Spectrom.*, 202, 91-109, 2000.
- 9 Chen, G., Davis, D., Crawford, J., Hutterli, L. M., Huey, L. G., Slusher, D., Mauldin, L.,
10 Eisele, F., Tanner, D., Dibb, J., Buhr, M., McConnell, J., Lefer, B., Shetter, R., Blake, D.,
11 Song, C. H., Lombardi, K., and Arnoldy, J.: A reassessment of HO_x South Pole chemistry
12 based on observations recorded during ISCAT 2000, *Atmos. Environ.*, 38, 5451-5461, 2004.
- 13 Crawford, J. H., Davis, D. D., Chen, G., Buhr, M., Oltmans, S., Weller, R., Mauldin, L.,
14 Eisele, F., Shetter, R., Lefer, B., Arimoto, R., and Hogan, A.: Evidence for photochemical
15 production of ozone at the South Pole surface, *Geophys. Res. Lett.*, 28, 3641-3644, 2001.
- 16 Davis, D., Nowak, J. B., Chen, G., Buhr, M., Arimoto, R., Hogan, A., Eisele, F., Mauldin, L.,
17 Tanner, D., Shetter, R., Lefer, B., and McMurry, P.: Unexpected high levels of NO observed
18 at South Pole, *Geophys. Res. Lett.*, 28, 3625-3628, 2001.
- 19 Davis, D. D., Eisele, F., Chen, G., Crawford, J., Huey, G., Tanner, D., Slusher, D., Mauldin,
20 L., Oncley, S., Lenschow, D., Semmer, S., Shetter, R., Lefer, B., Arimoto, R., Hogan, A.,
21 Grube, P., Lazzara, M., Bandy, A., Thornton, D., Berresheim, H., Bingemer, H., Hutterli, M.,
22 McConnell, J., Bales, R., Dibb, J., Buhr, M., Park, J., McMurry, P., Swanson, A., Meinardi,
23 S., and Blake, D.: An overview of ISCAT 2000, *Atmos. Environ.*, 38, 5363-5373, 2004.
- 24 Davis, D. D., Seelig, J., Huey, G., Crawford, J., Chen, G., Wang, Y. H., Buhr, M., Helmig,
25 D., Neff, W., Blake, D., Arimoto, R., and Eisele, F.: A reassessment of Antarctic plateau
26 reactive nitrogen based on ANTO 2003 airborne and ground based measurements, *Atmos.*
27 *Environ.*, 42, 2831-2848, 2008.
- 28 Dibb, J. E., Huey, L. G., Slusher, D. L., and Tanner, D. J.: Soluble reactive nitrogen oxides at
29 South Pole during ISCAT 2000, *Atmos. Environ.*, 38, 5399-5409, 2004.

1 Dusanter, S., Vimal, D., and Stevens, P. S.: Technical note: Measuring tropospheric OH and
2 HO₂ by laser-induced fluorescence at low pressure. A comparison of calibration techniques,
3 *Atmos. Chem. Phys.*, 8, 321-340, 2008.

4 Eisele, F. L. and Tanner, D. J.: Ion-Assisted Tropospheric OH Measurements, *J. Geophys.*
5 *Res. Atmos.*, 96, 9295-9308, 1991.

6 Eisele, F., Davis, D. D., Helmig, D., Oltmans, S. J., Neff, W., Huey, G., Tanner, D., Chen, G.,
7 Crawford, J., Arimoto, R., Buhr, M., Mauldin, L., Hutterli, M., Dibb, J., Blake, D., Brooks, S.
8 B., Johnson, B., Roberts, J. M., Wang, Y. H., Tan, D., and Flocke, F.: Antarctic Tropospheric
9 Chemistry Investigation (ANTCI) 2003 overview, *Atmospheric Environment*, 42, 2749-2761,
10 2008.

11 Faloon, I. C., Tan, D., Leshner, R. L., Hazen, N. L., Frame, C. L., Simpas, J. B., Harder, H.,
12 Martinez, M., Di Carlo, P., Ren, X. R., and Brune, W. H.: A laser-induced fluorescence
13 instrument for detecting tropospheric OH and HO₂: Characteristics and calibration, *J. Atmos.*
14 *Chem.*, 47, 139-167, 2004.

15 France, J. L., King, M. D., Frey, M. M., Erbland, J., Picard, G., Preunkert, S., MacArthur, A.,
16 and Savarino, J.: Snow optical properties at Dome C (Concordia), Antarctica; implications for
17 snow emissions and snow chemistry of reactive nitrogen, *Atmos. Chem. and Phys.*, 11, 9787-
18 9801, 2011.

19 Frey, M. M., Stewart, R. W., McConnell, J. R., and Bales, R. C.: Atmospheric hydroperoxides
20 in West Antarctica: Links to stratospheric ozone and atmospheric oxidation capacity, *J.*
21 *Geophys. Res. Atmos.*, 110, 2005.

22 Frey, M. M., Brough, N., France, J. L., Anderson, P. S., Traulle, O., King, M. D., Jones, A.
23 E., Wolff, E. W., and Savarino, J.: The diurnal variability of atmospheric nitrogen oxides (NO
24 and NO₂) above the Antarctic Plateau driven by atmospheric stability and snow emissions,
25 *Atmos. Chem. Phys.*, 13, 3045-3062, 2013.

26 Fuchs, H., Holland, F., and Hofzumahaus, A.: Measurement of tropospheric RO₂ and HO₂
27 radicals by a laser-induced fluorescence instrument, *Rev. of Sci. Instrum.*, 79, 2008.

28 Gallée, H. and Gorodetskaya, I.: Validation of a limited area model over Dome C, Antarctic
29 Plateau, during winter, 34, 61–72, *Clim. Dyn.*, doi:10.1007/s00382-008-0499-y, 2008.

1 Grannas, A. M., Jones, A. E., Dibb, J., Ammann, M., Anastasio, C., Beine, H. J., Bergin, M.,
2 Bottenheim, J., Boxe, C. S., Carver, G., Chen, G., Crawford, J. H., Domine, F., Frey, M. M.,
3 Guzman, M. I., Heard, D. E., Helmig, D., Hoffmann, M. R., Honrath, R. E., Huey, L. G.,
4 Hutterli, M., Jacobi, H. W., Klan, P., Lefer, B., McConnell, J., Plane, J., Sander, R., Savarino,
5 J., Shepson, P. B., Simpson, W. R., Sodeau, J. R., von Glasow, R., Weller, R., Wolff, E. W.,
6 and Zhu, T.: An overview of snow photochemistry: evidence, mechanisms and impacts,
7 *Atmos. Chem. Phys.*, 7, 4329-4373, 2007.

8 Hamer, P. D., Shallcross, D. E. and Frey, M. M.: Modelling the impact of oxygenated VOC
9 and meteorology upon the boundary layer photochemistry at the South Pole, *Atmos. Sci. Let.*,
10 8, 14-20, 2007.

11 Hanke, M., Uecker, J., Reiner, T., and Arnold, F.: Atmospheric peroxy radicals: ROXMAS, a
12 new mass-spectrometric methodology for speciated measurements of HO₂ and Sigma RO₂
13 and first results, *Int. J. Mass Spectrom.*, 213, 91-99, 2002.

14 Heard, D. E. and Pilling, M. J.: Measurement of OH and HO₂ in the troposphere, *Chem. Rev.*,
15 103, 5163-5198, 2003.

16 Heland, J., Kleffmann, J., Kurtenbach, R., and Wiesen, P. : A new instrument to measure
17 gaseous nitrous acid (HONO) in the atmosphere, *Environ. Sci. Technol.*, 35(15), 3207-3212,
18 doi:10.1021/es000303t, 2001.

19 Honrath, R. E., Peterson, M. C., Guo, S., Dibb, J. E., Shepson, P. B., and Campbell, B.:
20 Evidence of NO_x production within or upon ice particles in the Greenland snowpack, *Geophys.*
21 *Res. Lett.*, 26, 695-698, 1999.

22 Jäkel, E., Wendisch, M., Blumthaler, M., Schmitt, R., and Webb, A. R.: (2007). "A CCD
23 Spectroradiometer for Ultraviolet Actinic Radiation Measurements." *J. Atmos. Oceanic*
24 *Technol.* 24(3), 449-462.

25 Jenkin, M. E., Saunders, S. M., and Pilling, M. J.: The tropospheric degradation of volatile
26 organic compounds: A protocol for mechanism development, *Atmos. Environ.*, 31, 81-104,
27 1997.

28 Jones, A.E., Weller, R., Anderson, P.S., Jacobi, H.W., Wolff, E.W., Schrems, O., and Miller, H. :
29 Measurements of NO_x emissions from the Antarctic snowpack, *Geophys. Res. Lett.*, 28, 1499–1502,
30 2001.

1 Kerbrat, M., Legrand, M., Preunkert, S., Gallee, H., and Kleffmann, J.: Nitrous acid at
2 Concordia (inland site) and Dumont d'Urville (coastal site), East Antarctica, *J. Geophys. Res.*
3 *Atmos.*, 117, 2012.

4 King, J. C., Argentini, S. A., and Anderson, P. S.: Contrasts between the summertime surface
5 energy balance and boundary layer structure at Dome C and Halley stations, Antarctica, *J.*
6 *Geophys. Res. Atmos.*, 111, D02105, doi:10.1029/2005JD006130, 2012.

7 Kleffmann, J., Heland, J., Kurtenbach, R., Lorzer, J., and Wiesen, P.: A new instrument
8 (LOPAP) for the detection of nitrous acid (HONO), *Environ. Sci. Pollut. Res.*, (Sp. Iss. 4),
9 48–54, 2002.

10 Kukui, A., Ancellet, G., and Le Bras, G.: Chemical ionisation mass spectrometer for
11 measurements of OH and Peroxy radical concentrations in moderately polluted atmospheres,
12 *J. Atmos. Chem.*, 61, 133-154, 2008.

13 Kukui, A., Legrand, M., Ancellet, G., Gros, V., Bekki, S., Sarda-Estève, R., Loisil, R., and
14 Preunkert, S.: Measurements of OH and RO₂ radicals at the coastal Antarctic site of Dumont
15 d'Urville (East Antarctica) in summer 2010-2011, *J. Geophys. Res. Atmos.*, 117, 2012.

16 Legrand, M., Preunkert, S., Jourdain, B., Gallee, H., Goutail, F., Weller, R., and Savarino, J.:
17 Year-round record of surface ozone at coastal (Dumont d'Urville) and inland (Concordia) sites
18 in East Antarctica, *J. Geophys. Res. Atmos.*, 114, 2009.

19 Legrand, M., Gros, V., Preunkert, S., Sarda-Estève, R., Thierry, A.-M., Pépy, G., and
20 Jourdain, B.: A reassessment of the budget of formic and acetic acids in the boundary layer at
21 Dumont d'Urville (coastal Antarctica): The role of penguin emissions on the budget of several
22 oxygenated volatile organic compounds, *J. Geophys. Res. Atmos.*, 117, D06308,
23 doi:10.1029/2011JD017102, 2012.

24 Legrand, M., Preunkert, S., Frey, M., Bartels-Rausch, T., Kukui, A., King, M., Kerbrat, M.,
25 Jourdain, B., and Savarino, J.: High atmospheric levels of nitrous acid at Concordia (East
26 Antarctic plateau) in summer: A strong source from surface snow ?, *Atmos. Chem. Phys.*, this
27 issue.

28 Li, X., Rohrer, F., Hofzumahaus, A., Brauers, T., Häseler, R., Bohn, B., Broch, S., Fuchs, H.,
29 Gomm, S., Holland, F., Jäger, J., Kaiser, J., Keutsch, F. N., Lohse, I., Lu, K., Tillmann, R.,
30 Wegener, R., Wolfe, G. M., Mentel, T. F., Kiendler-Scharr, A., and Wahner, A.: Missing Gas-

- 1 Phase Source of HONO Inferred from Zeppelin Measurements in the Troposphere, *Science*,
2 344, 292-296, 2014.
- 3 Liao, J., Huey, L. G., Tanner, D. J., Brough, N., Brooks, S., Dibb, J. E., Stutz, J., Thomas, J.
4 L., Lefer, B., Haman, C., and Gorham, K.: Observations of hydroxyl and peroxy radicals and
5 the impact of BrO at Summit, Greenland in 2007 and 2008, *Atmos. Chem. Phys.*, 11, 8577-
6 8591, 2011.
- 7 Madronich, S.: Photodissociation in the atmosphere 1. Actinic flux and the effects of ground
8 reflectance and clouds, *J. Geophys. Res.* 92(D8), 9740-9752, 1987.
- 9 Madronich, S. and Flocke, S.: The role of solar radiation in atmospheric chemistry, in
10 *Handbook of Environmental Chemistry* (P. Boule, ed.), Springer_Verlag, Heidelberg, pp. 1-
11 26, 1998.
- 12 Mauldin, R. L., Eisele, F. L., Tanner, D. J., Kosciuch, E., Shetter, R., Lefer, B., Hall, S. R.,
13 Nowak, J. B., Buhr, M., Chen, G., Wang, P., and Davis, D.: Measurements of OH, H₂SO₄,
14 and MSA at the South Pole during ISCAT, *Geophys. Res. Lett.*, 28, 3629-3632, 2001.
- 15 Mauldin, R. L., Kosciuch, E., Henry, B., Eisele, F. L., Shetter, R., Lefer, B., Chen, G., Davis,
16 D., Huey, G., and Tanner, D.: Measurements of OH, HO₂+RO₂, H₂SO₄, and MSA at the
17 south pole during ISCAT 2000, *Atmos. Environ.*, 38, 5423-5437, 2004.
- 18 Mauldin, R., Kosciuch, E., Eisele, F., Huey, G., Tanner, D., Sjostedt, S., Blake, D., Chen, G.,
19 Crawford, J., and Davis, D.: South Pole Antarctica observations and modeling results: New
20 insights on HO_x radical and sulfur chemistry, *Atmos. Environ.*, 44, 572-581, 2010.
- 21 Michoud, V., Kukui, A., Camredon, M., Colomb, A., Borbon, A., Miet, K., Aumont, B.,
22 Beekmann, M., Durand-Jolibois, R., Perrier, S., Zapf, P., Siour, G., Ait-Helal, W., Locoge,
23 N., Sauvage, S., Afif, C., Gros, V., Furger, M., Ancellet, G., and Doussin, J. F.: Radical
24 budget analysis in a suburban European site during the MEGAPOLI summer field campaign,
25 *Atmos. Chem. Phys.*, 12, 11951-11974, 2012.
- 26 Neff, W., Helmig, D., Grachev, A., and Davis, D.: A study of boundary layer behavior
27 associated with high NO concentrations at the South Pole using a minisodar, tethered balloons
28 and sonic anemometer, *Atmos. Environ.*, 42, 2762-2779, 2008.

1 Novelli, P. C. and Masarie, K. A.: Atmospheric Carbon Monoxide Dry Air Mole Fractions
 2 from the NOAA ESRL Carbon Cycle Cooperative Global Air Sampling Network, 1988-2012,
 3 Version: 2013-06-18, Path: ftp://aftp.cmdl.noaa.gov/data/trace_gases/co/flask/surface/, 2013.

4 Preunkert, S., Ancellet, G., Legrand, M., Kukui, A., Kerbrat, M., Sarda-Estève, R., Gros, V.,
 5 and Jourdain, B.: Oxidant Production over Antarctic Land and its Export (OPALE) project:
 6 An overview of the 2010-2011 summer campaign, *J. Geophys. Res. Atmos.*, 117, 2012.

7 Preunkert, S., Legrand, M., Pépy, G., Gallée, H., Jones, A., and Jourdain, B.: The
 8 atmospheric HCHO budget at Dumont d'Urville (East Antarctica): Contribution of
 9 photochemical gas-phase production versus snow emissions, *J. Geophys. Res. Atmos.*, 118,
 10 doi:10.1002/2013JD019864, in press, 2014.

11 Preunkert, S., Legrand, M., Jourdain, B., Kukui, A., Gallée, H., and Frey, M.: Formaldehyde
 12 in air, snow, and interstitial air at Concordia (East Antarctic plateau), *Atmos. Chem. Phys.*,
 13 this issue.

14 Reiner, T., Hanke, M., and Arnold, F.: Atmospheric peroxy radical measurements by ion
 15 molecule reaction mass spectrometry: A novel analytical method using amplifying chemical
 16 conversion to sulfuric acid, *J. Geophys. Res. Atmos.*, 102, 1311-1326, 1997.

17 Sander, S. P., Abbatt, J., Barker, J. R., Burkholder, J. B., Friedl, R. R., Golden, D. M., Huie,
 18 R. E., Kolb, C. E., Kurylo, M. J., Moortgat, G. K., Orkin, V. L., and Wine, P. H.: Chemical
 19 Kinetics and photochemical Data for Use in Atmospheric Studies, Evaluation No. 17, JPL
 20 Publication 10-6, Jet Propulsion Laboratory, Pasadena, 2011 <http://jpldataeval.jpl.nasa.gov>.

21 Saunders, S. M., Jenkin, M. E., Derwent, R. G., and Pilling, M. J.: Protocol for the
 22 development of the Master Chemical Mechanism, MCM v3 (Part A): tropospheric
 23 degradation of non-aromatic volatile organic compounds, *Atmos. Chem. Phys.*, 3, 161-180,
 24 2003.

25 Sjostedt, S. J., Huey, L. G., Tanner, D. J., Peischl, J., Chen, G., Dibb, J. E., Lefer, B., Hutterli,
 26 M. A., Beyersdorf, A. J., Blake, N. J., Blake, D. R., Sueper, D., Ryerson, T., Burkhardt, J., and
 27 Stohl, A.: Observations of hydroxyl and the sum of peroxy radicals at Summit, Greenland
 28 during summer 2003, *Atmos. Environ.*, 41, 5122-5137, 2007.

29 Slusher, D. L., Huey, L. G., Tanner, D. J., Chen, G., Davis, D. D., Buhr, M., Nowak, J. B.,
 30 Eisele, F. L., Kosciuch, E., Mauldin, R. L., Lefer, B. L., Shetter, R. E., and Dibb, J. E.:

1 Measurements of pernitric acid at the South Pole during ISCAT 2000, *Geophys. Res. Lett.*,
2 29, 2002.

3 Slusher, D. L., Neff, W. D., Kim, S., Huey, L. G., Wang, Y., Zeng, T., Tanner, D. J., Blake,
4 D. R., Beyersdorf, A., Lefer, B. L., Crawford, J. H., Eisele, F. L., Mauldin, R. L., Kosciuch,
5 E., Buhr, M. P., Wallace, H. W., and Davis, D. D.: Atmospheric chemistry results from the
6 ANTCI 2005 Antarctic plateau airborne study, *J. Geophys. Res. Atmos.*, 115, 2010.

7 Steele, L. P., Krummel, P. B. and Langenfelds, R. L.: Atmospheric H₂ concentrations from
8 sites in the CSIRO Atmospheric Research GASLAB air sampling network (October 2002
9 version). In *Trends: A Compendium of Data on Global Change, Carbon Dioxide Information*
10 *Analysis Center*, Oak Ridge National Laboratory, U.S. Department of Energy, Oak Ridge,
11 TN, U.S.A., 2003.

12 Steele, L. P., Krummel, P. B. and Langenfelds, R. L.: Atmospheric CH₄ concentrations from
13 sites in the CSIRO Atmospheric Research GASLAB air sampling network (October 2002
14 version). In *Trends: A Compendium of Data on Global Change, Carbon Dioxide Information*
15 *Analysis Center*, Oak Ridge National Laboratory, U.S. Department of Energy, Oak Ridge,
16 TN, U.S.A., 2002.

17 Tanner, D. J., Jefferson, A., and Eisele, F. L.: Selected ion chemical ionization mass
18 spectrometric measurement of OH, *J. Geophys. Res. Atmos.*, 102, 6415-6425, 1997.

1

2 **Table 1.** Comparison of measurements at Dome C and at the South Pole

	Dome C, 75.1° S / 123.3° E 19 Dec, 2011 ÷ 10 Jan, 2012		SP, ISCAT 1998	SP, ISCAT 2000	SP, ANTICI 2003
	Median (range of median) values	Method (2σ uncertainty)	Median values (Dec, 16-31) ^{a)}		
P, mb	645		688	692	695
T, °C	-29.6 (-35.8 ÷ -26.1)		-29.1	-27.6	-23.9
WS, m s ⁻¹	3.1 (2.3÷4.5)		3.2	3.74	4.9
OH, 10 ⁶ molecule cm ⁻³	3.1 (1.1÷5.0) 5.0 (at 12h, JO ¹ D=5×10 ⁻⁵) 2.5 (at 5h, JO ¹ D=9×10 ⁻⁶) 3.8 (at 19h, JO ¹ D=9×10 ⁻⁶)	CIMS (40% - 60%)	1.7	2.3	1.2
RO ₂ , 10 ⁷ molecule cm ⁻³	9.9 (2.5÷17.0) 17.0 (at 12h, JO ¹ D=5×10 ⁻⁵) 7.9 (at 5h, JO ¹ D=9×10 ⁻⁶) 7.5 (at 19h, JO ¹ D=9×10 ⁻⁶)	CIMS (47% - 50%)	-	8.1	-
J(O ¹ D), 10 ⁻⁶ s ⁻¹	13.4 (1.2 ÷ 49)	Spectroradiometer (MetCon ...) (3% (JNO ₂); 6% (JO ¹ D))	8.9	8.5	8.5
J(NO ₂), 10 ⁻² s ⁻¹	1.3 (0.4 ÷ 2.1)		1.0	1.1	0.8
O ₃ , ppb	23.7 (22÷25)	UV abs. (2%)	26.1	30	32
NO, ppt (1m)	77 (46÷134)	Chemiluminescence (40%) ^{h)}	237	88	76
NO ₂ , ppt (1m)	149 (110÷239) 16 (7-64) ⁱ⁾	Photolytic conv., Chemiluminescence (200%) ^{h)}	115 ^{b)}	44 ^{b)}	38 ^{b)}
HONO, ppt	38 (27÷44)	LOPAP (5%)	-	28 (MC/IC)	4.9 (LIF, 10m) 51(MC/IC, 1m) ^{c)} 7.3 (LIF, 10m) ^{c)}
HCHO, ppt	131 (117÷153)	Fluorimetry, Aerolaser AL4021 (20%)	-	105	74
H ₂ O ₂ , ppt	166 (128÷228)	Fluorimetry, Aerolaser AL2021 (18%)	-	229	286
P(O ₃), ppb day ⁻¹	4.7 (0.04 ÷ 0.34, in ppb h ⁻¹) ^{d)}		2.2÷3.6 ^{e)}	3.2÷4.8 ^{f)}	1÷3.5 ^{g)}

3

4 a) SP data from (Eisele et al., 2008), if no other reference

5 b) estimated assuming PSS ratio NO/NO₂=2 (Davis et al., 2004; Slusher et al., 2002);

6 c) median for 1-15 of December

7 d) calculated using the measured RO₂ and NO

8 e) Crawford et al., (2001)

9 f) Chen et al., (2004)

10 g) Davis et al., (2008)

11 h) median of relative 2σ errors

12 i) NO₂ estimated assuming photostationary steady-state conditions for NO_x

1 **Table 2.** Sources and sinks of OH and RO₂ radicals estimated from the measurements available at Dome C ^{*)}

		<i>net OH sources</i>		
		<i>median rate, 10⁵ molecule cm⁻³s⁻¹</i>		
		<i>daily</i>	<i>noon</i>	<i>midnight</i>
1	HONO+hν → OH + NO	14.2 (0.5)	21.8 (0.6)	4.7 (0.2)
2	H ₂ O ₂ +hν → OH + OH	0.9	2.1	0.1
3	O ₃ + hν → O(¹ D) → OH + OH	0.3	1.7	0.0
4	CH ₃ OOH + hν → HO ₂ + OH	0.2	0.4	0.0
		<i>recycling RO₂ → OH</i>		
5	HO ₂ + NO → OH + NO ₂	8.3	11.6	2.2
6	HO ₂ + O ₃ → OH + 2O ₂	0.4	0.6	0.1
		<i>net RO₂ sources</i>		
7	HCHO + hν → 2HO ₂ + CO	2.1	3.7	0.4
8	CH ₃ CHO + hν → HO ₂ + CH ₃ O ₂ + CO	0.9	2.1	0.2
9	CH ₃ OOH + hν → HO ₂ + OH	0.2	0.4	0.03
		<i>recycling OH → RO₂</i>		
10	CO + OH → HO ₂ + CO ₂	5.9	7.8	1.9
11	CH ₄ + OH → CH ₃ O ₂ + H ₂ O	2.3	3.3	0.7
12	HCHO + OH → HO ₂ + CO	1.0	1.1	0.3
13	CH ₃ CHO + OH → CH ₃ CO ₃	0.8	1.1	0.3
14	O ₃ + OH → HO ₂ + O ₂	0.6	0.7	0.2
15	H ₂ + OH → HO ₂ + H ₂ O	0.5	0.8	0.2
16	CH ₃ OOH + OH → CH ₃ O ₂ + H ₂ O	0.3	0.5	0.1
17	H ₂ O ₂ + OH → HO ₂ + H ₂ O	0.1	0.3	0.0
		<i>net radical losses</i>		
18	OH + NO ₂ → HNO ₃	1.9 (0.3)	2.2 (0.3)	1.1 (0.3)
19	OH + NO → HONO	0.5	0.6	0.2
20	OH + RO ₂ → products	0.4	1.0	0.0
21	OH + RO ₂ NO ₂ → products	0.4 (0.05)	0.5 (0.06)	0.1 (0.02)
22	OH + HONO → H ₂ O + NO ₂	0.1 (0.0)	0.2 (0.0)	0.1 (0.0)
23	OH + HNO ₃ → H ₂ O + NO ₃ ^{a)}	0.0	0.0	0.0
24	RO ₂ + NO ₂ → RO ₂ NO ₂ → products	1.9 (0.3)	2.4 (0.3)	1.2 (0.3)
25	RO ₂ + RO ₂ → products	0.7	2.1	0.1
26	RO ₂ + OH → products	0.4	1.0	0.0
Σ OH sources		24.2 ± 2.1 ^{b)} (10.6 ± 0.2)	38.3 ± 3.2 (17.1±0.3)	7.1 ± 0.7 (4.3±0.1)
Σ OH losses		14.8 ± 4.6 (12.9±1.8)	20.3 ± 3.6 (17.9±2.2)	5.1 ± 1.2 (4.3±0.9)
Δ		9.4 ± 5.0 (-2.4±2.7)	17.9 ± 4.8 (-0.8±3.8)	2.1 ± 1.4 (-1.7±1.2)
Σ RO ₂ sources		14.6 ± 1.8	21.9 ± 2.3	4.2 ± 0.9
Σ RO ₂ losses		11.7 ± 4.6 (10.2±2.1)	17.7 ± 7.2 (15.6±3.3)	3.5 ± 1.6 (2.7±0.8)
Δ		2.9 ± 5.0 (4.4±2.8)	4.2 ± 7.6 (6.3±4.0)	0.7 ± 1.9 (1.5±1.2)
Σ RO ₂ and OH net sources		18.7 ± 0.6 (5.1±0.3)	32.3 ± 0.9 (11.1±0.7)	5.5 ± 0.1 (0.9±0.1)
Σ RO ₂ and OH net losses		6.4 ± 5.9 (3.0±0.8)	10.1 ± 7.1 (5.6±1.1)	2.7 ± 1.7 (1.1±0.4)
Δ		12.3 ± 6.0 (2.1±0.9)	22.2 ± 7.2 (5.5±1.3)	2.7 ± 1.7 (-0.1±0.5)
$P_{pr}^{net}(OH) = \Sigma net OH sources - \Sigma net OH losses$		12.2 ± 4.2 (0.4±0.3)	21.4 ± 3.0 (2.7±0.5)	3.4 ± 0.8 (-0.3±0.2)
$R_{net}(OH \rightarrow RO_2) = \Sigma(OH \rightarrow RO_2) - \Sigma(RO_2 \rightarrow OH)$		2.8 ± 2.7	3.5 ± 3.8	1.4 ± 1.1
$P_{pr}^{net}(RO_2) = \Sigma net RO_2 sources - \Sigma net RO_2 losses$		0.15 ± 4.2 (1.7±0.8)	0.74 ± 6.6 (2.8±1.2)	-0.7 ± 1.5 (0.2±0.4)

2 ^{*)} Values in parentheses correspond to NO₂ and HONO estimated assuming PSS

3 ^{a)} HNO₃ of (100±30) ppt was assumed (Slusher et al., 2010)

4 ^{b)} 1σ uncertainty estimated with accounting for measurement uncertainties

1
2
3
4
5
6
7
8
9
10
11
12

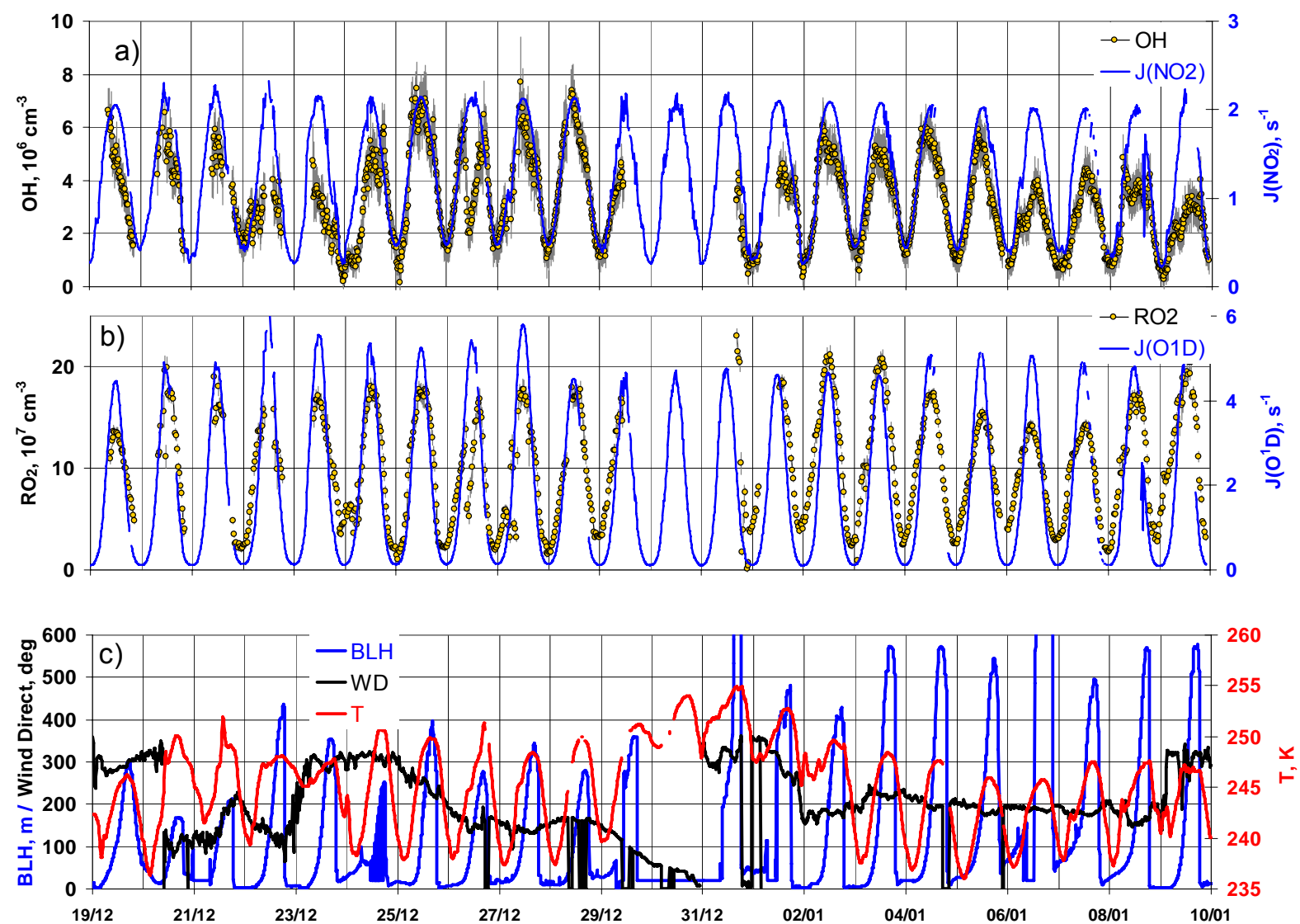


Figure 1. Temporal profiles at Dome C: $[\text{OH}]$, $J(\text{NO}_2)$ (a); $[\text{RO}_2]$, $J(\text{O}^1\text{D})$ (b); Wind Direction, temperature and modelled Boundary Layer Height (BLH) (c).

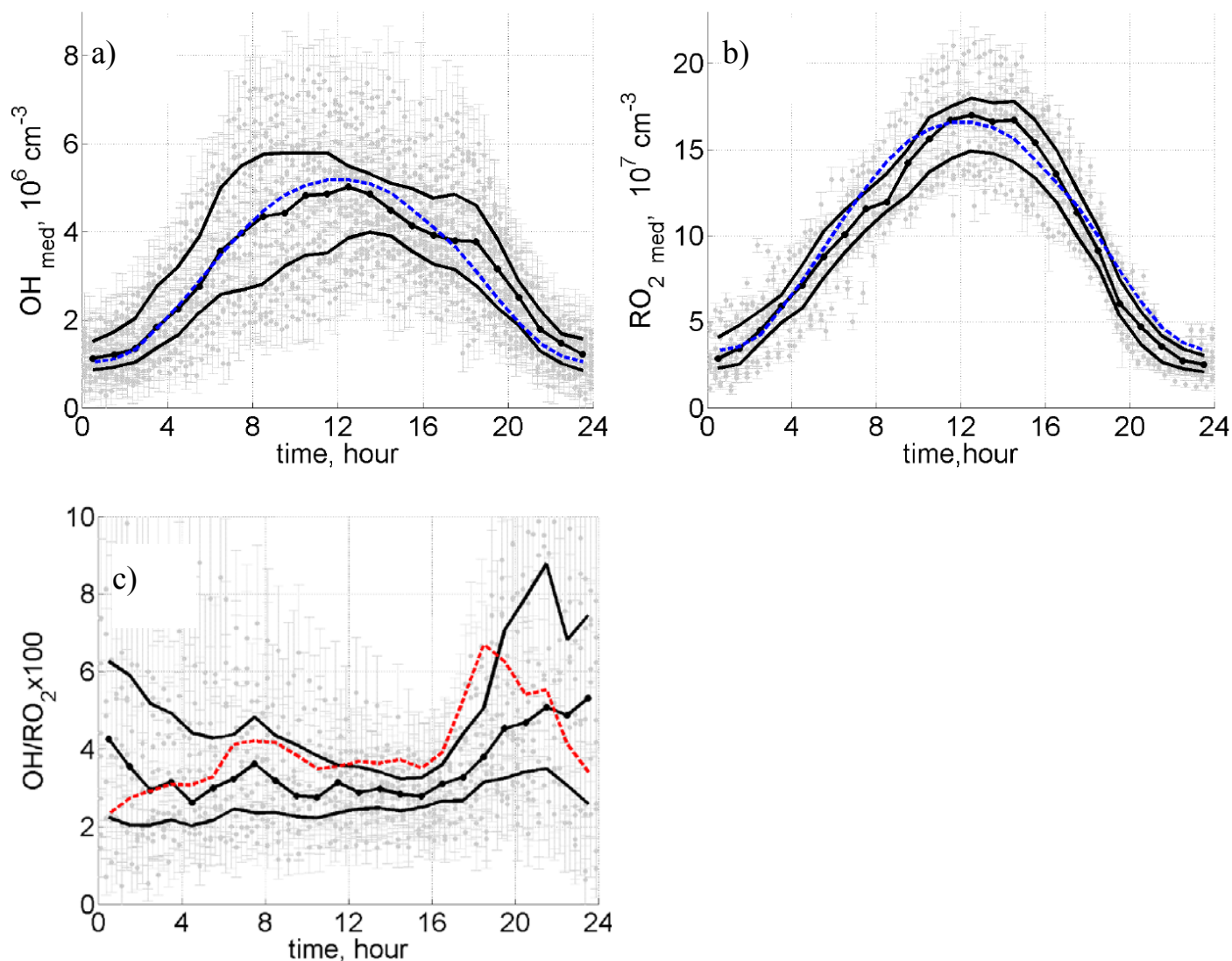


Figure 2. Median diurnal concentration profiles of OH (a), RO_2 (b), $[\text{OH}]/[\text{RO}_2]$ ratio (c). Solid lines represent the median and quartile levels. Points – 15 min averaged measured values with standard deviations. Blue line on a) and b) represents $J(\text{NO}_2)$ in arbitrary units. Red line on c) represents median NO.

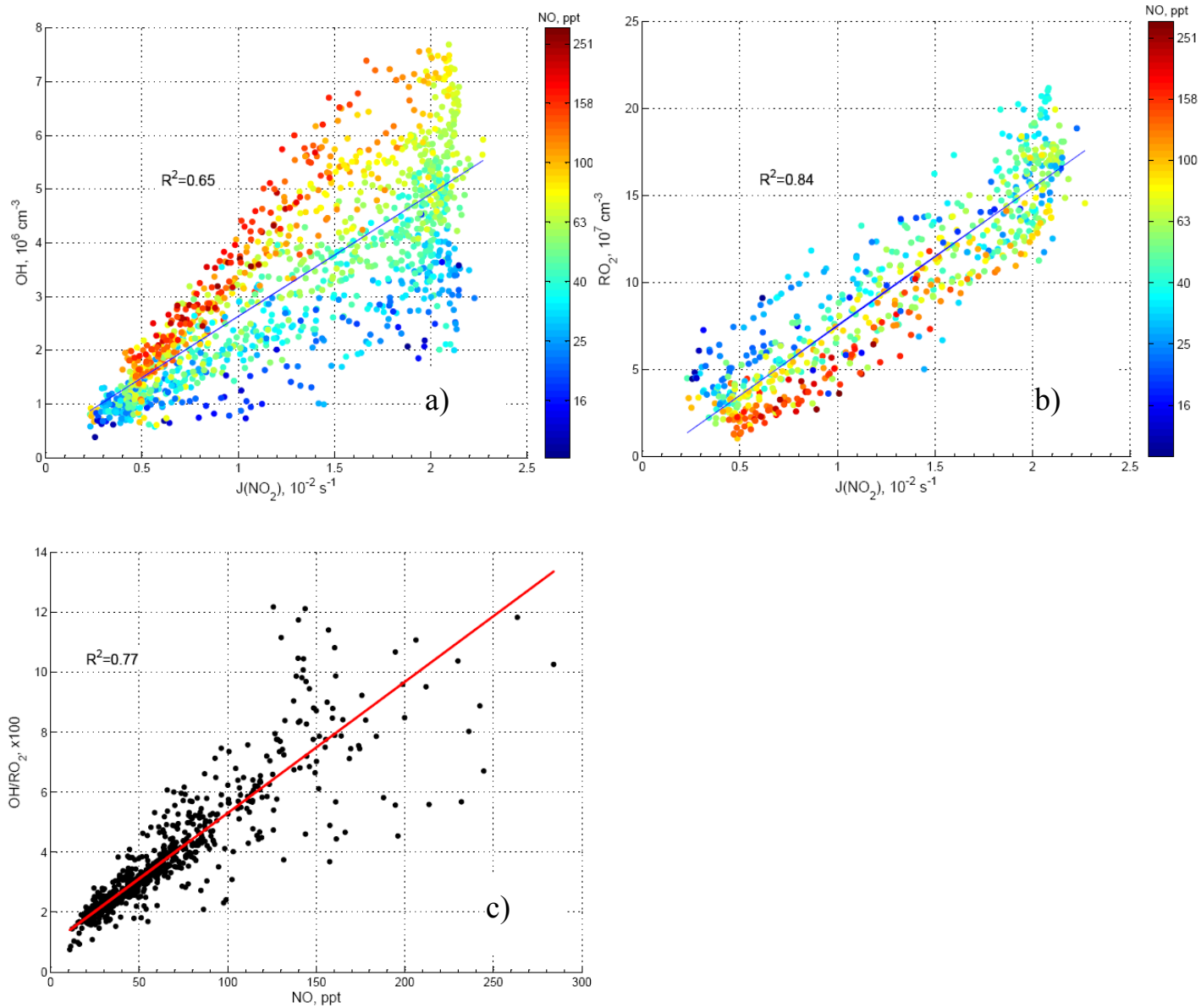


Figure 3. Correlations of $[\text{OH}]$ (a) and $[\text{RO}_2]$ (b) with $J(\text{NO}_2)$ and of $[\text{OH}]/[\text{RO}_2]$ with $[\text{NO}]$ (c).

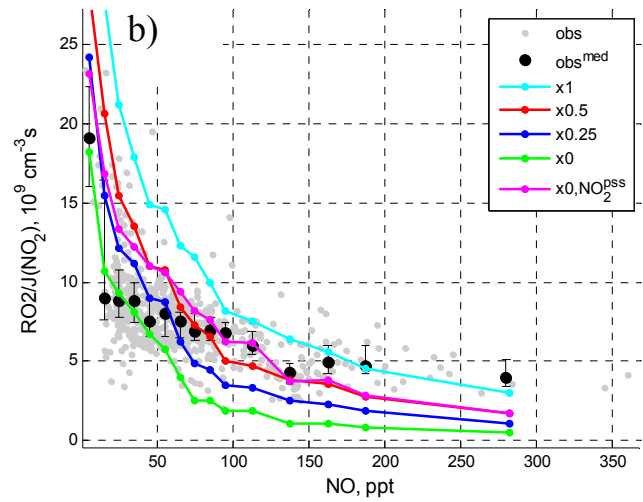
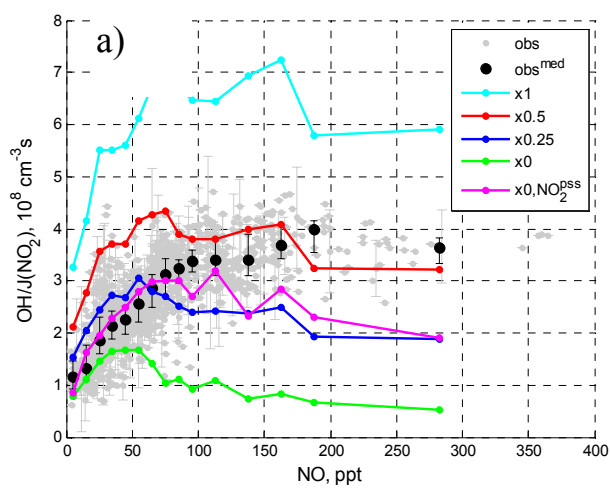
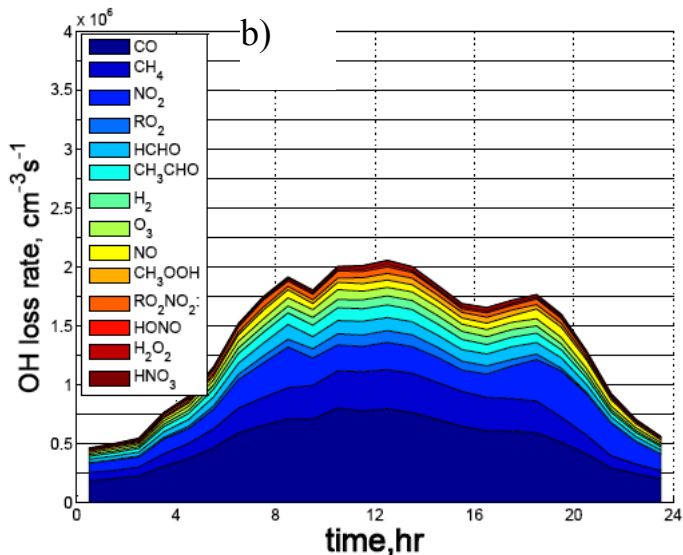
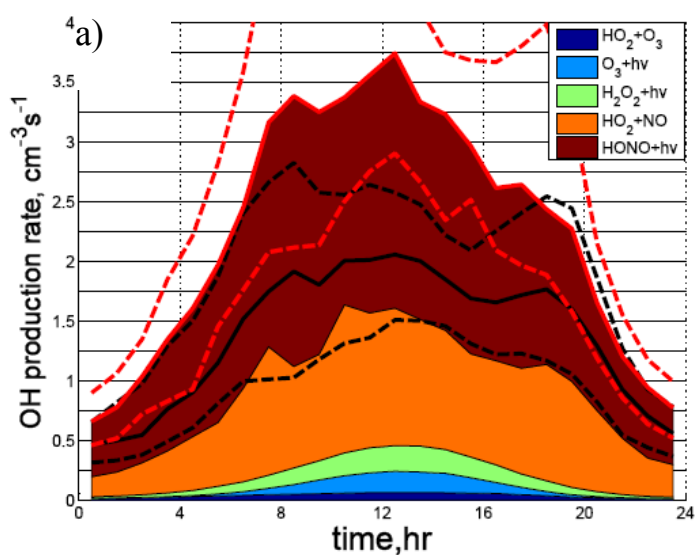
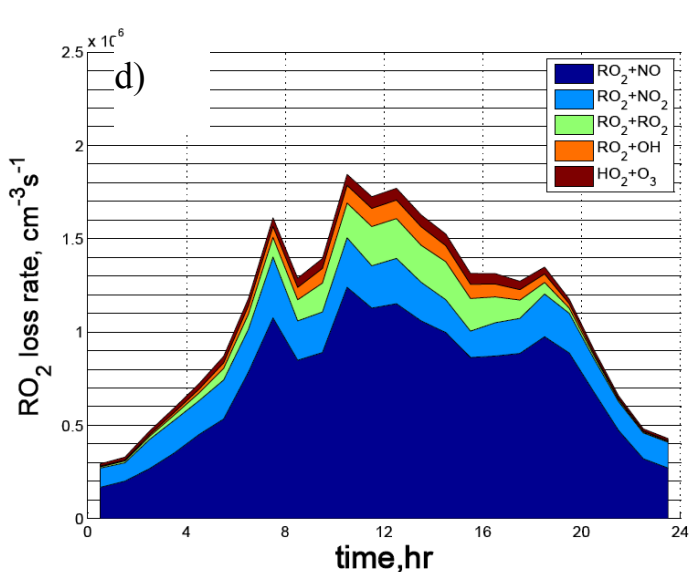
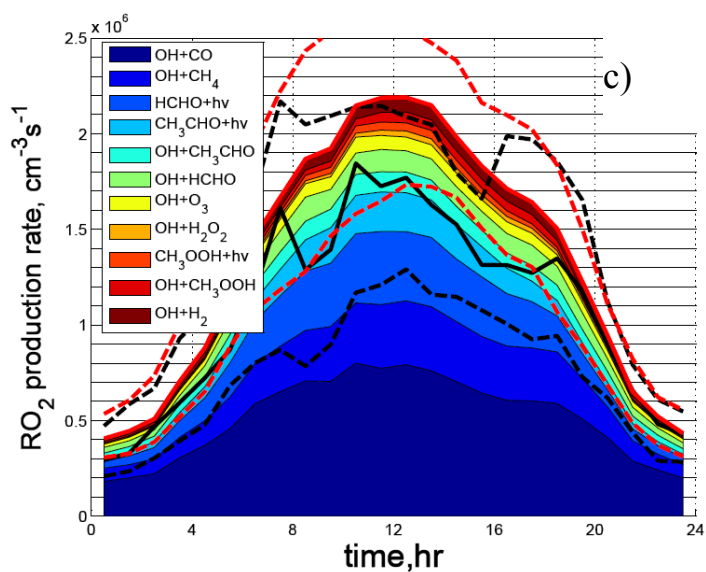


Figure 4. Normalized concentrations of OH (a) and RO₂ (b) versus measured concentrations of NO. Grey and black points represent observations; colored lines – MCM calculations with [HONO] multiplied by a factor presented in Figure legends (x0 corresponds to estimated steady-state HONO concentrations). Magenta – [HONO]=0 and [NO₂] is calculated by assuming PSS [NO₂]/[NO] ratio.

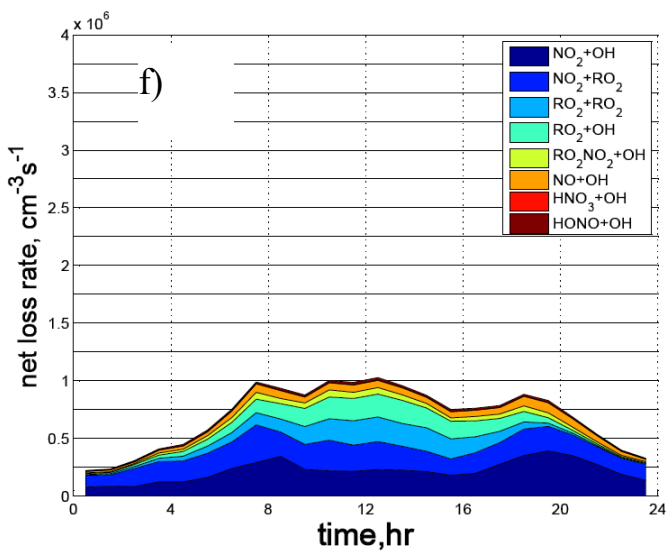
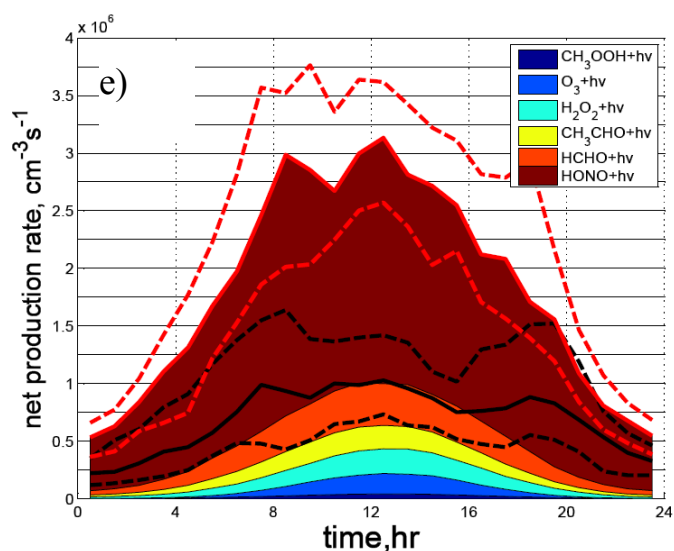
1



2



3



4

5

6

Figure 5. Median diurnal production and loss rates of OH (a,b), RO₂(c,d); net production and loss rates of radicals (e,f). Solid red and black lines represent the total production and loss rates, respectively. Dashed lines correspond to corresponding quartiles.

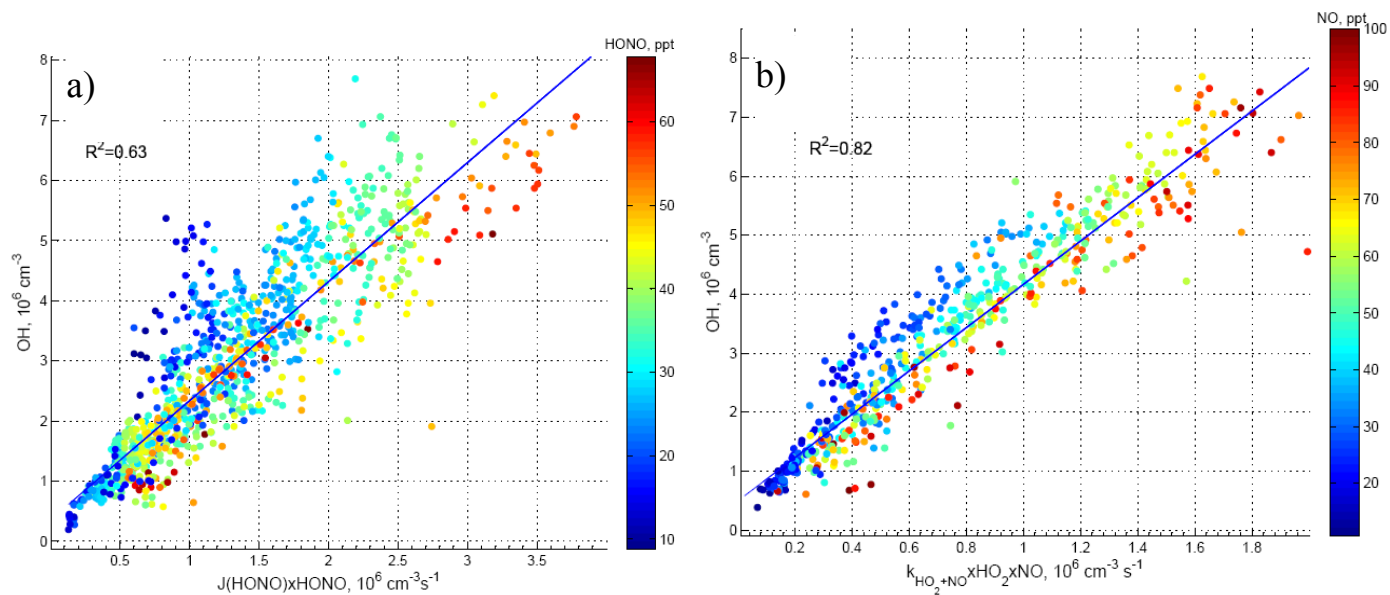


Figure 6. Correlation of measured $[\text{OH}]$ with production rates of OH radical by photolysis of HONO, P_{HONO} , (a) and via reaction $\text{HO}_2 + \text{NO}$, $P_{\text{HO}_2+\text{NO}}$ (b).

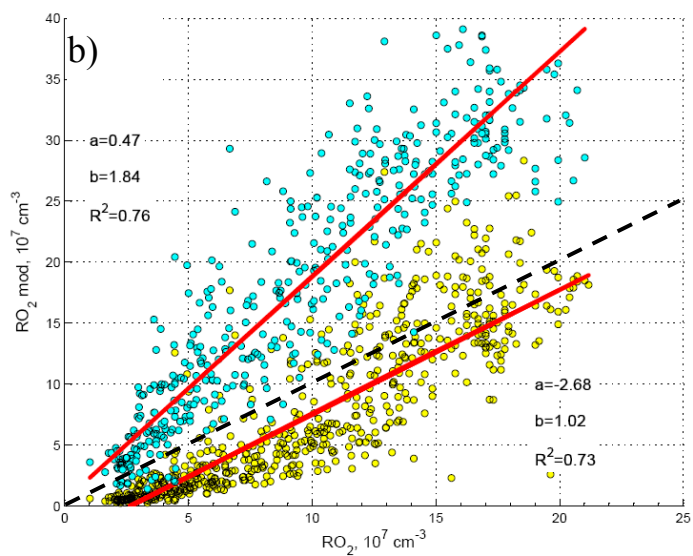
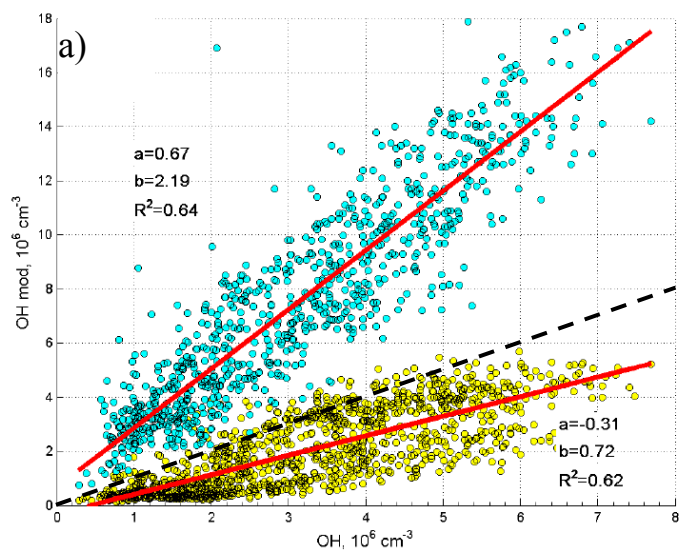


Figure 7. Modelled with the 0-D model vs measured [OH] (a) and [RO₂] (b): yellow – with PSS estimated HONO; blue – with measured [HONO]. Coefficients a,b correspond to intercept and slope, respectively. Black lines correspond to linear dependences with a=0 and b=1.

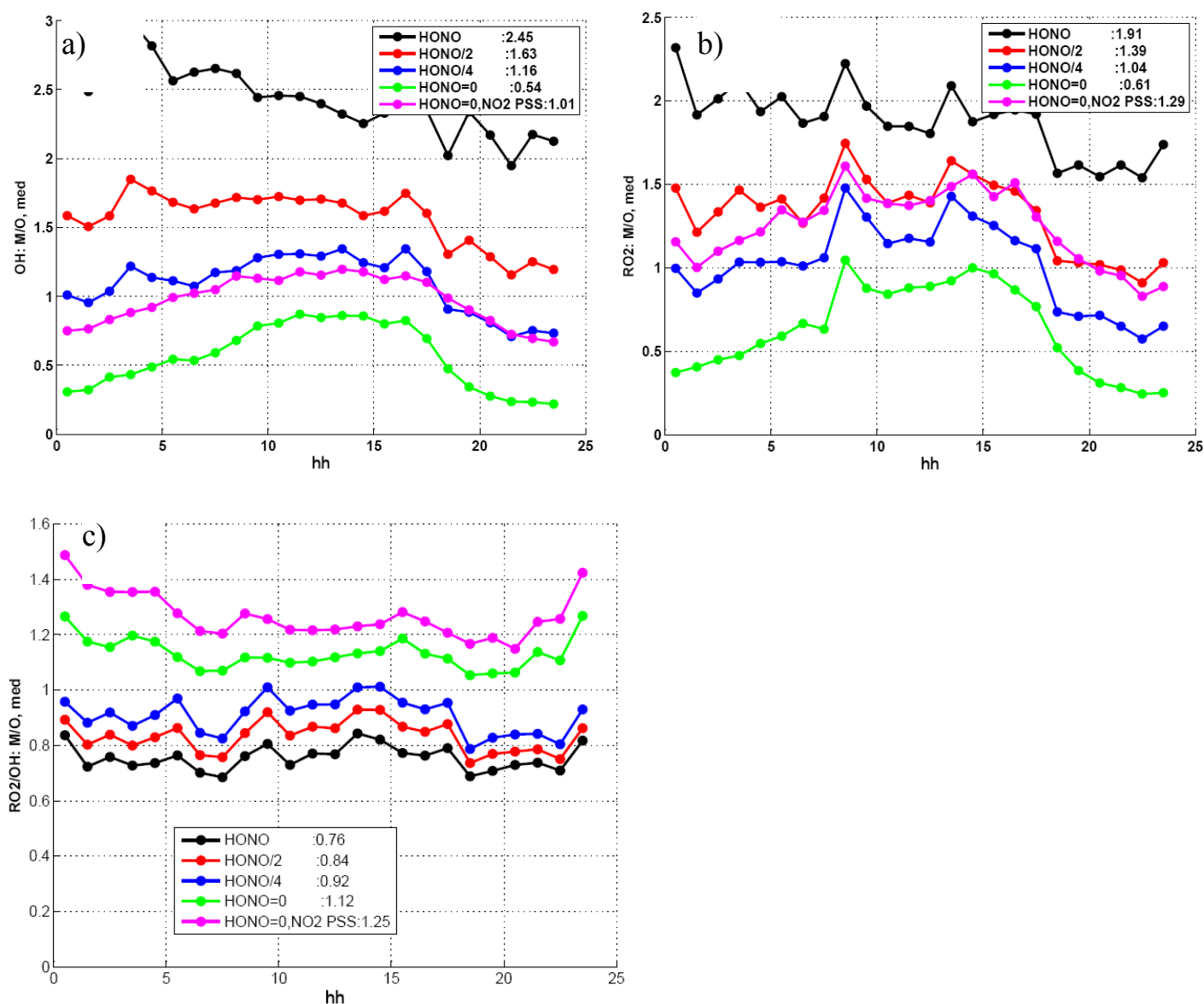


Figure 8. Median diurnal Model/Observation ratios for [OH], [RO₂] and [RO₂]/[OH] at [HONO]=1, 0.5, 0.25, of measured. The “HONO=0, NO₂ PSS” curves correspond to the model with [HONO] estimated assuming PSS and [NO₂] calculated assuming [NO_x] at PSS. Numbers in legends represent diurnal median M/O ratios.

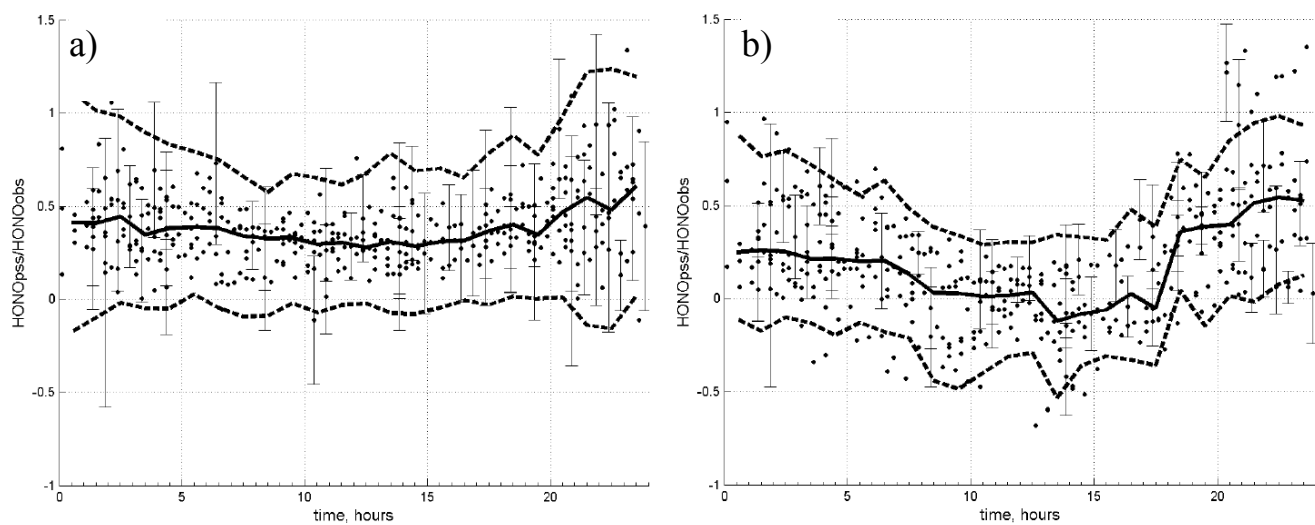


Figure 9. Ratio of PSS calculated and measured [HONO]: a) from OH budget; b) from net radical (OH and RO_2) sources and sinks. Solid lines – median values; dashed lines- upper and lower quartiles of the mean values with added and subtracted standard deviation, respectively. Error bars correspond to standard deviation.

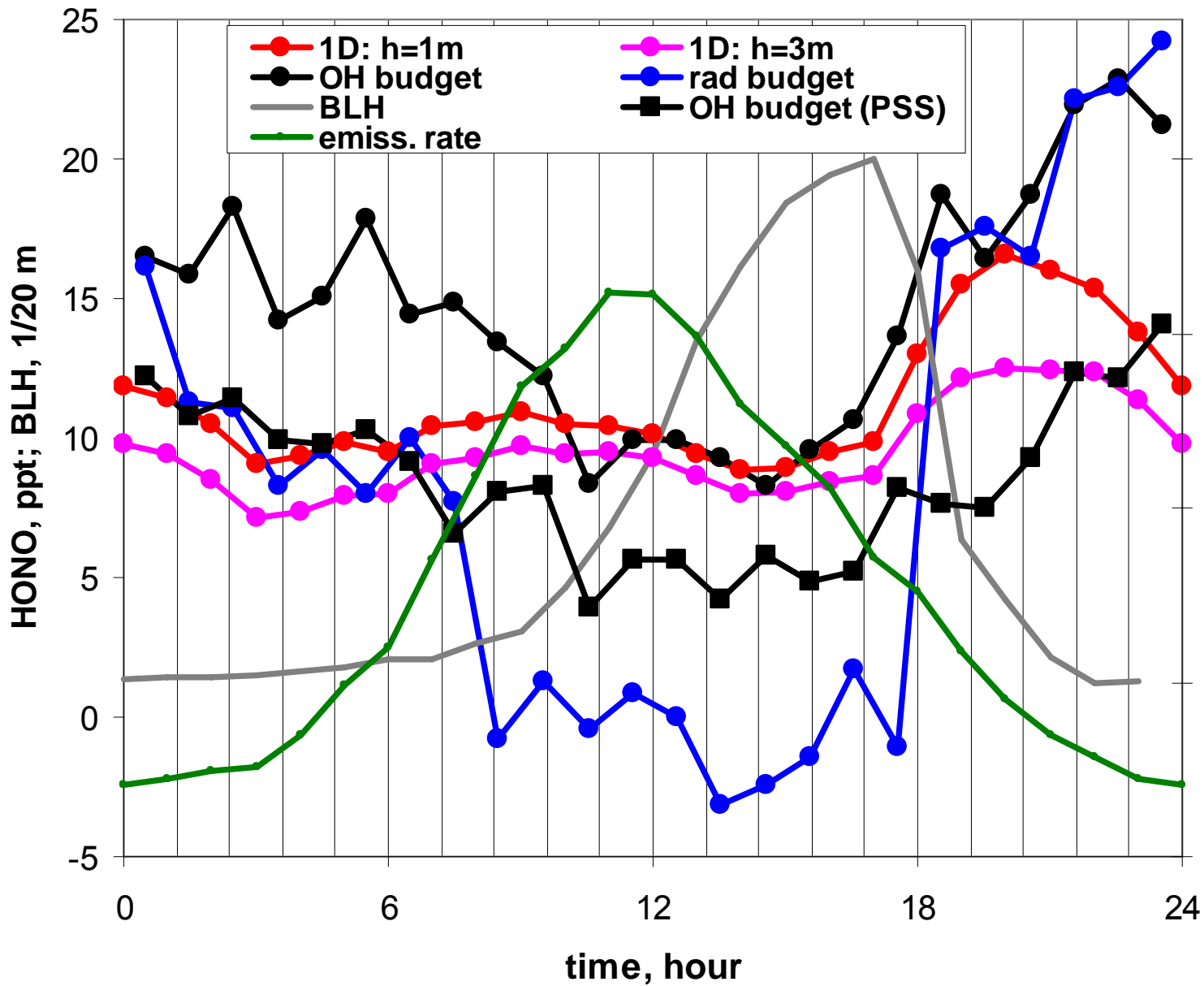


Figure 10. Comparison of median diurnal profiles of [HONO] derived from OH (black) and sum of radicals (OH and RO₂) (blue) budgets with [HONO] calculated with 1D model at the heights of 1m (red) and 3m (magenta) for the days 2-9 of January. Black circles and squares correspond to [HONO] derived using measured and calculated steady-state [NO₂], respectively. Grey and green lines represent modelled median boundary layer height and HONO emission rates, respectively.

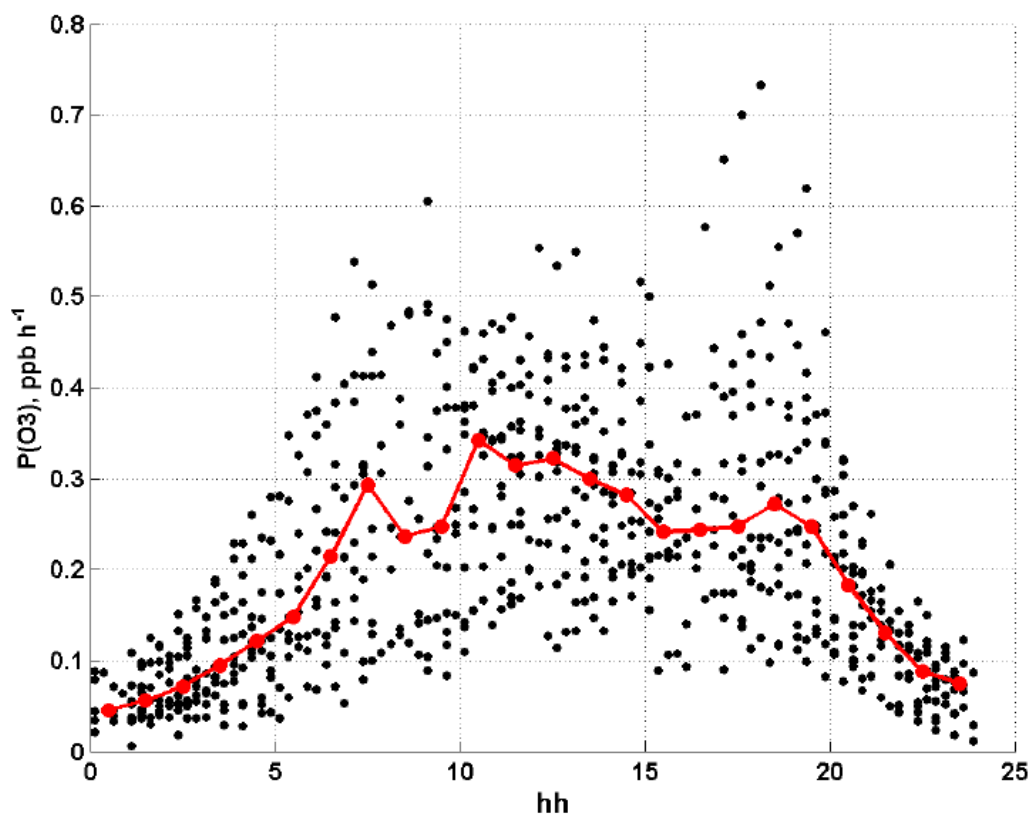


Figure 11. Ozone production calculated from measured $[RO_2]$ and $[NO]$: red line represents hourly median values.